J. Fluid Mech. (1992), *vol.* 244, *pp.* 405–436

Numerical simulations of Lewis number effects in turbulent premixed flames

By D. C. HAWORTH[1] AND T. J. POINSOT[2]†

[1]Thermosciences Department, General Motors Research Laboratories, Warren, MI 48090, USA

[2]Center for Turbulence Research, Stanford University, Stanford, CA 94305, USA

(Received 25 March 1991 and in revised form 30 March 1992)

The structure of a premixed flame front propagating in a region of two-dimensional turbulence is investigated using full numerical simulation including heat release, variable properties, and one-step Arrhenius chemistry. The influence of reactant Lewis number (Le = ratio of thermal to species diffusivity) is reported for $Le = 0.8$, $Le = 1.0$, and $Le = 1.2$ flames. Local flame behaviour is described by comparing the local instantaneous turbulent flame structure (local consumption rate of reactants) to the steady one-dimensional laminar flame structure for the same thermochemical parameters. Statistics of flame front strain rates and curvature are calculated and global quantities of interest in modelling (flame surface area, mean reactant consumption rate per unit area of flame, and turbulent flame speed) are reported. Principal findings are: that probability density functions (p.d.f.s) of flame curvature are nearly symmetric about a near-zero mean; that the flame tends to align preferentially with extensive tangential strain rates; that the local flame structure of the non-unity Lewis number flames correlates more strongly with local flame curvature than with tangential strain rate; that the mean consumption rate per unit area is relatively insensitive to curvature and is controlled by the mean tangential strain rate; and, that more flame area is generated for $Le < 1$ than for $Le > 1$. Implications of the results for flamelet models of turbulent premixed combustion are discussed.

1. Introduction

The structure of premixed flames in turbulent flows is an important fundamental and practical question in turbulent combustion. In applications such as reciprocating internal combustion engines, accurate modelling of turbulent premixed combustion is an essential step in formulating truly predictive multidimensional simulations that can be used to study aerothermochemical processes and to optimize designs.

Because flame structure information is difficult to obtain experimentally, numerical simulations have become an important tool in complementing experimental investigations of turbulent combustion. For the foreseeable future, numerical simulation of the full three-dimensional governing partial differential equations with variable density and transport properties and complex chemistry will remain intractable; thus various levels of simplification will remain necessary. On one hand, the requirement to simplify is not necessarily a handicap: numerical

† Present address: Laboratoire EM2C, CNRS, Ecole Centrale de Paris, 92295 Chatenay-Malabry, Cedex, France.

simulations allow the researcher a degree of control in isolating specific physical phenomena that is inaccessible in experiments. For example, one can 'turn off' heat release to study the influence of turbulence on chemical reaction without the confounding effects of chemistry on the flow field through density and fluid property variations. On the other hand, the highly coupled nonlinear nature of the governing partial differential equations demands that one remains wary when extrapolating results obtained in such idealized modelled systems to practical turbulent premixed flames.

In the present study, the modelled system includes heat release, variable fluid properties, and simple chemistry in two-dimensional turbulence. While it is recognized that two-dimensional turbulence differs from three-dimensional turbulence (e.g. Batchelor 1953; Herring *et al.* 1974; Lesieur 1987), it is our feeling that the response of the physical flame structure to straining and curvature should be generic even if detailed statistical correlations (especially of small-scale quantities) differ quantitatively from what would be found in three dimensions. Restricting the simulations to two dimensions also permits a wider dynamic range of scales to be computed so that, for example, higher-turbulence Reynolds numbers can be simulated while still resolving the flame structure. In any case, the present results can be compared with three-dimensional constant-density computations (e.g. El Tahry, Rutland & Ferziger 1991; Cant, Rutland & Trouvé 1990*b*; Rutland, Ferziger & El Tahry 1990; Rutland & Trouvé 1990) to understand better the limitations and similarities of the two approaches. Some comparisons of this kind are offered in what follows.

If chemical times are short enough compared to turbulence times, the flame zone is 'thin' and may be treated, in the limit, as a discontinuous interface separating fresh unburnt reactants from hot burnt products. The discontinuous interface model is valid only if the flame is thinner than any scale of turbulent motion. However, the concept of local laminar-like flame structure in turbulent premixed flames is appropriate well outside of this limit. For our purposes, we adopt the weak definition proposed by Poinsot, Veynante & Candel 1991: a turbulent premixed reacting flow is in a *flamelet* regime if any line connecting one point in the fresh gases to another point in the burnt products crosses at least one active flame front. The flamelet regime has been invoked widely as a framework for the construction of turbulent combustion models (e.g. Bray & Libby 1986; Candel *et al.* 1988; Pope & Cheng 1988; Cant & Bray 1988; Maistret *et al.* 1989; El Tahry 1990; Cant, Pope & Bray 1990*a*; Bray 1990). There are two quantities of primary importance for flamelet models: (i) the total flame surface (the area of the interface separating fresh and burnt gases); and, (ii) the local structure of the individual flamelets. Although these flame elements are thin, their internal structure is influenced by the flow characteristics and has an influence on the global consumption rate of reactants.

The objective of this work is to investigate the dependence of the local and global structure of premixed flames propagating into mixtures with non-unity Lewis number Le (Le = ratio of thermal to species diffusivities). The Lewis number has been identified in asymptotic analyses of laminar premixed flames as an important parameter influencing flame structure and stability (e.g. Williams 1985): we wish to assess its importance in turbulent flames.

The remainder of the paper is organized as follows. The following section contains a review of previous work on numerical simulations of turbulent premixed flames and the motivation for the present study. Section 3 provides an outline of the governing equations and numerical methods and a description of the diagnostics used to extract

the desired physical information from the simulations. Results are presented in §4. In §5, several aspects of the computations and results are discussed; this includes the foreseeable effects of complex chemistry, the relevance of molecular effects in high-Reynolds-number turbulent combustion, and implications of the parameter ranges that have been investigated. The results are summarized in §6. Definitions of relevant scales and details of diagnostics are given in the Appendix.

2. Background and motivation

The use of numerical simulation as a tool for investigating turbulent flame structure is reviewed briefly with particular attention to the merits and drawbacks of two-dimensional simulations. Lewis number effects in laminar premixed flames are summarized next to motivate the present study of non-unity Lewis numbers in turbulent premixed flames. Finally, the influence of curvature and strain rate on premixed flame fronts is discussed.

2.1. *Numerical simulations of turbulent premixed flames*

We limit our discussion to 'direct numerical simulations' (DNS), i.e. computations in which all scales of turbulent motion from the largest energy-containing scales to the smallest dissipative scales are fully resolved both spatially and temporally so that no turbulence modelling is used. Moreover, we are interested primarily in calculations in which the flame structure is resolved. This is in contrast to studies where the flame is treated as a propagating interface of infinitesimal thickness separating cold reactants from hot products (e.g. Kerstein, Ashurst & Williams 1988; Ashurst, Shivashinsky & Yakhot 1988; Ashurst 1990; Girimaji & Pope 1992). The interface, or flame sheet, type of calculations have added significantly to our understanding of flame topology and have provided quantitative information on statistical correlations that is useful in the construction of models of turbulent premixed combustion in the flamelet regime.

Studies of the dynamical interactions between fluid flow and finite-rate chemistry in flamelet or non-flamelet regimes, on the other hand, require that the flame structure be resolved. However, the addition of chemical lengthscales and timescales that are of the order of or smaller than the smallest fluid-mechanical scales implies that, for a given spatial and temporal resolution, a smaller range of hydrodynamic scales can be simulated compared to computations in which the flame has no internal structure. Two-dimensional vortex methods have been used to study interactions between turbulent fluid flow and finite-rate chemistry in a number of papers including those by Ashurst & Barr (1983), Ghoniem & Krishnan (1988), and Ashurst, Peters & Smooke (1987). The last of these deals with non-unity Lewis number flames and is thus of particular interest in the present study.

The first full three-dimensional simulations of premixed turbulent flames with finite-rate chemistry (constant density, zero heat release, single-step Arrhenius chemistry) have been reported by Rutland *et al.* (1990) (further results may be found in El Tahry *et al.* 1991). Among other things, their results included the distribution of local burning rate over a range of Damköhler numbers (ratio of a characteristic flow timescale to a characteristic chemical timescale) to assess the applicability of laminar flamelet models: at high Damköhler numbers, the local structure of the turbulent flame was found to be that of an unstrained steady laminar flame while at low Damköhler numbers, the local flame structure could not be correlated with that of a steady one-dimensional strained laminar flame. Further three-dimensional

constant-density simulations of premixed turbulent flames have been performed recently by Rutland & Trouvé (1990) (a study of Lewis number effects) and by Cant *et al.* (1990*b*) (a study of statistics relevant to the Bray–Moss–Libby model of turbulent premixed combustion; e.g. Bray & Libby 1986; Bray 1990). In all cases, the Taylor-scale Reynolds number Re_λ has been limited to the range $Re_\lambda \leqslant 20$.

A number of two-dimensional simulations including variable fluid properties and heat release have been reported recently by Poinsot and coworkers (Poinsot *et al.* 1990, 1991, 1992; Meneveau & Poinsot 1991). These studies include a characterization of the scales of turbulent motion that influence flame structure (Poinsot *et al.* 1990, 1991) and investigations of flame quenching (Poinsot *et al.* 1991; Meneveau & Poinsot 1991). The same two-dimensional code has been adopted for the present study. Compared to three-dimensional constant-property simulations, two-dimensional variable-density simulations allow a wider dynamic range of scales (higher Reynolds and Damköhler numbers) and full two-way fluid-chemistry coupling. Values of relevant dimensionless parameters in the present study are given in §3. However, the dynamics of two-dimensional turbulence are not identical to those of three-dimensional turbulence (Batchelor 1953; Herring *et al.* 1974; Lesieur 1987). In particular, the vortex-stretching mechanism for the cascade of energy to progressively smaller scales of motion is absent in two dimensions and the smallest scales of motion do not follow the usual Kolmogorov scaling. Instead, the microscales are based on the mean-square vorticity (enstrophy) and its dissipation rate.

Our emphasis in the present study is on flame structure. Relevance of the present results to three-dimensional turbulent premixed flames demands, for example, that the response of the flame to hydrodynamic straining be reasonably generic in both two and three spatial dimensions. This is less restrictive than requiring that flow dynamics and statistics of small-scale quantities be quantitatively the same in two- and in three-dimensional turbulence. Further justification for the appropriateness of two-dimensional studies of premixed flame structure can be found in recent three-dimensional (constant density) work (Ashurst 1990; Cant *et al.* 1990*b*; Girimaji & Pope 1992): the topology of a propagating surface in three-dimensional turbulence has been found to be primarily two-dimensional, particularly those surface elements having the highest curvatures. That is, a flame tends to be locally cylindrical rather than spherical in shape. Both two-dimensional and three-dimensional numerical simulations (and one-dimensional, when focusing on specific issues such as complex chemistry or radiation effects) will continue to be useful tools in fundamental studies of premixed combustion for some time to come.

2.2. *Lewis number effects in premixed flames*

We restrict our attention to a single-step reaction mechanism,

$$R \text{ (reactants)} \rightarrow P \text{ (products)}, \tag{1}$$

where the reaction rate $\dot{w}_R$ is given by an Arrhenius expression with activation temperature T_a,

$$\dot{w}_R = B\rho Y_R \exp\left(-\frac{T_a}{T}\right). \tag{2}$$

It is convenient to follow Williams (1985) and cast this expression in the form,

$$\dot{w} = \dot{w}_R / Y_{R1} = \mathscr{B}\rho\tilde{Y}\exp\left(\frac{-\beta(1-\Theta)}{1-\alpha(1-\Theta)}\right). \tag{3}$$

Here Θ is the reduced temperature, $\Theta = (T-T_1)/(T_2-T_1)$, where subscript '1' refers to the fresh gases and '2' to the burnt products (T_2 is the adiabatic flame temperature). The coefficients $\mathscr{B}$, α, and β are, respectively, the reduced pre-exponential factor, the temperature factor, and the reduced activation energy,

$$\mathscr{B} = B\exp(-\beta/\alpha), \quad \alpha = (T_2-T_1)/T_2, \quad \beta = \alpha T_a/T_2. \tag{4}$$

The mass fraction of the reactants Y_R has been non-dimensionalized by the initial mass fraction of reactants Y_{R1} in the fresh gases, $\tilde{Y} = Y_R/Y_{R1}$, so that $\tilde{Y}$ varies from unity in the fresh gases to zero in the burnt gases.

A normalized local flame speed in the turbulent flame (consumption speed or 'flamelet speed') s_l^* is defined by integrating the local reaction rate profile in a direction normal to the flame,

$$s_l^* = \int \dot{w}\,\mathrm{d}n/\rho_1 s_l^0 = s_l/s_l^0. \tag{5}$$

Here s_l^0 is the undisturbed laminar flame speed for a steady planar laminar flame having the same Lewis number.

Textbook discussions of thermodiffusive effects for premixed laminar flames reveal the following behaviour (e.g. Williams 1985). For $Le = 1$ (and subject to other assumptions consistent with those made above), the reaction rate is a unique function of the reactant mass fraction or temperature ($\Theta + \tilde{Y} = 1$ everywhere). Thus the maximum reaction rate along the normal to the flame is fixed: the local consumption speed is controlled only by the flame thickness, and its variations are expected to be small. Asymptotic analysis for small perturbations from a planar flame (Clavin 1985) reveals that flame curvature concave towards the products or positive (extensive) tangential strain rates can reduce the local speed of advance of the propagating flame relative to the fresh gases, and conversely for curvature concave towards reactants or compressive tangential strain rates.

For Lewis numbers other than unity, differential diffusion between heat and species leads to richer possibilities in flame structure. For $Le > 1$, elements of flame surface that are concave towards the reactants are expected to burn faster, while elements that are concave towards the products are expected to have a lower burning rate compared to that of a planar flame. Positive (extensive) tangential strain will decrease the flamelet speed relative to that of an undisturbed laminar flame for $Le > 1$. On the other hand, Lewis numbers less than unity display the opposite behaviour: lower burning rate for elements concave towards reactants; higher burning rates for elements concave towards products; and, increasing flamelet speed with extensive strain.

Ashurst *et al.* (1987) reported two-dimensional numerical simulations of premixed flames with non-unity Lewis numbers in the limit of zero heat release. The thermodiffusive effects described above for non-unity Lewis number were observed in their simulations. Results were expressed in terms of the excess enthalpy relative to an undisturbed laminar flame; a correlation between strain rate and excess enthalpy was reported. Here, we calculate cases with higher turbulence intensity (tables 1 and 4), variable properties, and heat release. The local flame structure is found to correlate more strongly with the local flame curvature than with strain rate, while global flame behaviour depends on both strain and curvature.

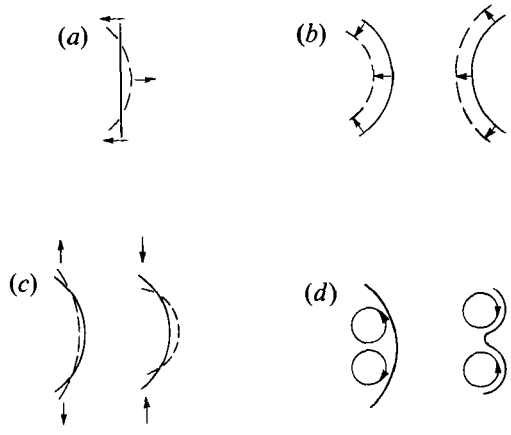

FIGURE 1. Mechanisms that modify the curvature of a propagating surface element (Pope 1988): (*a*) bending; (*b*) self-propagation; (*c*) stretching; (*d*) flow structures leading to strain rate–curvature correlation. For (*a*)–(*c*), ——, surface at time t_1; – – –, surface at time $t_2 > t_1$.

2.3. *Strain rate and curvature: propagating surfaces*

In the previous subsection, strain rate and curvature influences have been discussed from the point of view of thermochemical effects in laminar premixed flames. Further insight can be gained by considering the kinematics of a propagating surface in a turbulent flow (Pope 1988; Candel & Poinsot 1990). In both of these references is derived the relationship among the instantaneous rate-of-change of surface area A, the tangential strain rate a_t (equation (A 17)), and the local radius of curvature $\mathscr{R}$ (equation (A 15)):

$$\frac{1}{A}\frac{\mathrm{d}A}{\mathrm{d}t} = a_t + \frac{s_d}{\mathscr{R}}, \tag{6}$$

where s_d is the speed of advance of the propagating surface relative to the fresh gases (the displacement speed; Poinsot, Echekki & Mungal 1992). The first term on the right-hand side reflects the rate of area increase through hydrodynamic straining: extensive tangential strains act to increase the surface area and conversely for compressive strains. The second term represents the change in area of a propagating curved surface: the area decreases for propagation towards the centre of curvature ($\mathscr{R} < 0$ in the present convention) and increases for propagation away from the centre.

Equation (6) applies rigorously only for an infinitesimal propagating surface. For a non-zero-thickness flame, the question is approximate and the location at which to evaluate a_t, $\mathscr{R}$, and s_d is not well defined. Nevertheless, this equation expresses the fundamental dependence of flame area on strain rate and curvature and motivates attempts to isolate strain effects from curvature effects on premixed flame structure.

In fact, strain rate and curvature are not independent quantities. An equation governing the evolution with time of the curvature of a surface element propagating with constant speed has been derived by Pope (1988). This equation reveals three effects that modify surface element curvature: (i) an initially planar surface develops non-zero curvature through straining (bending); (ii) the curvature of an initially curved surface changes because of self-propagation (this is the dominant term at large curvatures and can lead to infinite curvatures, or cusps); and (iii) stretching (tangential strain) of an initially curved surface modifies its curvature. These three

effects are sketched in figure 1. We will return to this sketch later in §4. Even though curvature is tied to strain through a differential equation, it is of interest to assess the relative contribution of strain rate versus curvature in influencing the local and global characteristics of the turbulent flame. This is useful both for physical understanding and from a modelling point of view.

3. Problem definition

In this section, the governing equations, numerical methods, and computational configuration are summarized. Ranges of dimensionless parameters characterizing the computations are tabulated and discussed. In the final subsection, the diagnostics used to extract physical information from the numerical solution are described.

3.1. *Governing equations and numerical methods*

The set of equations solved is the compressible flow equations comprising conservation of mass, linear momentum, energy, and reactant mass fraction. In Cartesian tensor notation,

$$\frac{\partial \rho}{\partial t}+\frac{\partial \rho u_i}{\partial x_i}=0, \tag{7}$$

$$\frac{\partial \rho u_i}{\partial t}+\frac{\partial \rho u_i u_j}{\partial x_j}=-\frac{\partial p}{\partial x_i}+\frac{\partial \tau_{ij}}{\partial x_j}, \tag{8}$$

$$\frac{\partial \rho E}{\partial t}+\frac{\partial (\rho E+p)\, u_i}{\partial x_i}=\frac{\partial (u_j \tau_{ij})}{\partial x_i}+\frac{\partial}{\partial x_i}\left(\lambda \frac{\partial T}{\partial x_i}\right)+Q\dot{w}, \tag{9}$$

$$\frac{\partial \rho \tilde{Y}}{\partial t}+\frac{\partial \rho \tilde{Y} u_i}{\partial x_i}=\frac{\partial}{\partial x_i}\left(\rho \mathscr{D} \frac{\partial \tilde{Y}}{\partial x_i}\right)-\dot{w}. \tag{10}$$

Here u_i is the ith component of the fluid velocity, $\tilde{Y}$ is the normalized reactant mass fraction defined earlier, ρ is the fluid density, p is the thermodynamic pressure, and Q is the heat of reaction per unit mass of fresh mixture ($Q=-\Delta h_f^0 Y_{R1}$, where Δh_f^0 is the heat of reaction per unit mass of reactant). The total energy density per unit volume is ρE, and τ_{ij} us the viscous stress tensor,

$$\rho E=\tfrac{1}{2}(\rho u_k u_k)+\frac{p}{\gamma-1}, \tag{11}$$

$$\tau_{ij}=\mu\left(\frac{\partial u_i}{\partial x_j}+\frac{\partial u_j}{\partial x_i}-\tfrac{2}{3}\delta_{ij}\frac{\partial u_k}{\partial x_k}\right). \tag{12}$$

The Arrhenius reaction scheme is defined by (1)–(4); this can be interpreted as a binary reaction where one of the reactants is always deficient.

Fluid density follows an ideal gas equation of state with constant molar mass and constant specific heat ratio γ. The molecular transport coefficients (viscosity μ, thermal conductivity λ, and species diffusion coefficient $\mathscr{D}$) depend on temperature in such a way that the Prandtl number Pr and Lewis number Le are constant,

$$\rho=\rho_1(pT_1/p_1T),\quad \mu=\mu_1(T/T_1)^b,\quad \lambda=\mu c_p/Pr,\quad \mathscr{D}=\mu/(\rho LePr). \tag{13}$$

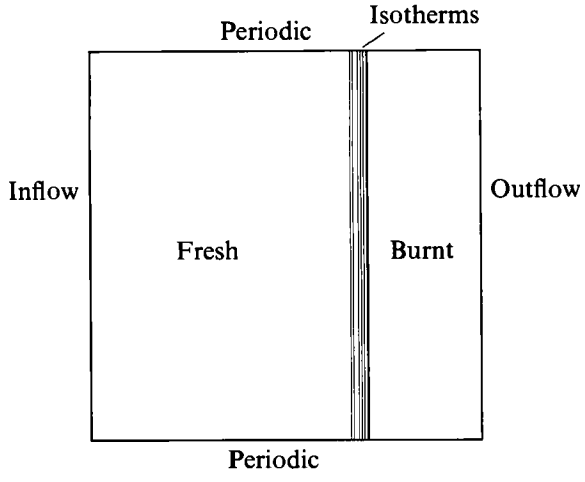

FIGURE 2. Schematic of two-dimensional computational configuration and the initial planar flame.

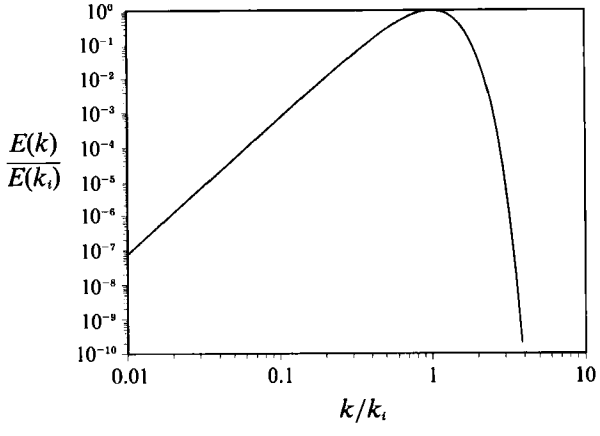

FIGURE 3. Normalized initial energy spectrum $E(k)/E(k_i)$ (equation 14) with $u_p = 0.1$, $L_t = 0.7$.

Using these assumptions and a Cartesian frame of reference, the governing equations are solved using a high-order finite difference scheme. The numerical accuracy is sixth-order in space and third-order in time (Lele 1990). Spatial derivatives are computed using a compact scheme and the time advancement is produced by a minimal-storage third-order Runge–Kutta method (Wray 1990). Boundary conditions are specified using the NSCBC method (Poinsot & Lele 1992). Further details concerning the system of equations solved and the numerical methods can be found in these papers. Typical grids contain 400^2 grid points.

A schematic of the rectangular computational domain is given in figure 2. The left- and right-hand sides of the box are inflow and outflow boundaries, respectively, while periodic boundary conditions are specified at the top and bottom. The calculations are initialized with reactants on one side of the box and products on the other; the two are separated by a planar laminar premixed flame. The initial velocity field (turbulence spectrum) is specified at $t = 0$ and the system is allowed to evolve in time. The initially planar flame is convected and strained by the turbulence while the

Case	Le	u_p/s_l^0	L_t/δ_{th}	t/τ_0	u'/s_l^0	l/δ_{th}	Re_t	τ/τ_f	u_η/s_l^0	l_η/δ_{th}	τ_η/τ_f	l_η/l_k	τ_η/τ_k
1*b*	0.8	6.60	4.27	1.95	4.82	3.60	86	0.74	0.87	0.24	0.28	1.49	2.23
2*b*	1.0	6.28	4.46	1.96	4.68	4.00	91	0.86	0.82	0.25	0.30	1.48	2.20
3*b*	1.2	5.84	4.82	1.96	4.32	4.26	88	0.99	0.76	0.27	0.36	1.48	2.20

TABLE 1. Dimensionless parameters for three primary cases at dimensionless time $t/\tau_0 \approx 2.0$, where τ_0 is the initial turbulence eddy turnover time

combustion influences the fluid mechanics through dilatation and temperature-dependent properties (equation (13)).

The initial velocity field is homogeneous and isotropic in the cold reactants with a two-parameter (r.m.s. velocity u_p and peak energy wavelength L_i) energy spectrum $E(k)$, k being the wavenumber:

$$E(k) = \tfrac{32}{3}(2/\pi)^{\frac{1}{2}} u_p^2/k_i (k/k_i)^4 \exp\{-2(k/k_i)^2\} \quad (k_i = 2\pi/L_i). \tag{14}$$

This spectrum is sketched in figure 3. There the principal features of (14) are evident: $E(k) \sim k^4$ for $k \ll k_i$; $E(k)_{\max} = E(k_i)$; and, $E(k) \sim \exp\{-2k^2\}$ for $k \gg k_i$. The results have been found to be insensitive to the initial post-flame turbulence specification, as the temperature-dependent viscosity largely suppresses turbulent velocity fluctuations in the hot products.

3.2. *Scales and dimensionless parameters*

Relevant scales for this problem are defined in the Appendix. Three kinds of scales are introduced: scales characteristic of the energy-containing turbulent motions u', l, and τ ((A 1)–(A 5)); scales characteristic of the smallest turbulent motions u_η, l_η, and τ_η (enstrophy-based, (A 10)) and u_k, l_k, and τ_k (Kolmogorov microscales, (A 11)); and, chemical scales s_l^0, δ_{th}, and τ_f ((A 12)–(A 14)). All turbulence scales have been calculated as volume-averaged quantities conditioned on being in the fresh reactants ahead of the flame. Unambiguous definition of a length scale l characteristic of the energy-containing motions is problematic in view of the non-equilibrium two-dimensional nature of the turbulence. The value adopted (equation (A 5)) is $l = 0.42 l_\epsilon = 0.42 u'^3/\epsilon$. This choice allows direct comparison with turbulence model (e.g. $k-\epsilon$) results, and is in most cases close to the value based on two-point velocity correlations (equation (A 4)). Kolmogorov scales are reported for comparison purposes only: these are not expected to represent the smallest scales of motion in two-dimensional turbulence. Chemical scales are based on the speed and thickness (defined using the temperature profile) of an undisturbed steady planar laminar flame at the same Lewis number as the turbulent flame.

The values of various dimensionless combinations of scales for the three runs that are the focus of the present study are reported in table 1. These three runs are (initially) identical except for the Lewis number; that is, the same flow realization has been used as the initial condition for all three. The flames of table 1 have evolved for about two turbulence eddy turnover times. Table 4 is similar, summarizing all runs that have been analysed. While the bulk of our analysis and discussion is based on the runs of table 1, any differences or interesting features that result from the different parameter ranges in table 4 will be noted as appropriate. Except as so noted, it may be assumed that conclusions drawn from Cases 1b, 2b and 3b are supported by the results of the other runs as well. Chemical and fluid parameters that have been held fixed for all runs are given in table 2.

α	β	$\mathscr{B}$	b	Pr	λ
0.75	8.00	146	0.76	0.75	1.4

TABLE 2. Fixed parameters for all cases

Some comments on the regime of combustion implied by the parameters of tables 1, 2, and 4 are appropriate. It can be seen in table 1 that at $t/\tau_0 \approx 2.0$, these three runs are in a regime where the turbulence is intense relative to the laminar flame speed ($u'/s_l^0 \approx 5$), the flame is thin compared to the largest turbulent lengthscales but is thicker than the smallest ($l/\delta_{ll} \approx 4$, $l_\eta/\delta_{ll} \approx 0.3$), and chemical times are of the order of the longest turbulence timescales ($\tau/\tau_t \approx 1$) and are three to four times longer than the shortest turbulence timescales ($\tau_\eta/\tau_t \approx 0.3$–$0.4$). Turbulence Reynolds numbers Re_l are close to 100, giving a range of scales of motion of $l/l_\eta \approx 15$. The ratio of the smallest hydrodynamic velocity scale to the undisturbed laminar flame speed is $u_\eta/s_l^0 \approx 0.8$–0.9. The enstrophy-based microscales are somewhat larger than the Kolmogorov scales by a ratio of about 1.5 for lengthscales and 2.2 for timescales.

The critical Lewis number Le_c for diffusive-thermal instability can be estimated using the formula derived for a single-reactant system with constant specific heats and subject to other assumptions as enumerated, for example in Williams (1985):

$$Le_c = 1 - \beta^{-1}\left\{2R_0 \ln(R_0) \Big/ \int_0^{R_0-1} x^{-1}\ln(1+x)\,dx\right\}.$$

Here R_0 is the density ratio and β is the reduced activation energy (equation (4)). For the present $\beta = 8$ and $R_0 = 4$, $Le_c \approx 0.385$. Thus the three Lewis numbers considered (0.8, 1.0, and 1.2) all lie above Le_c.

The ranges of scales for all runs and their evolution with time can be seen in table 4. In general, the turbulence velocity scale u' decays slowly over the course of a run while the lengthscale l grows somewhat faster so that $\tau = l/u'$ and the Reynolds number Re_l increase with time; in low u' cases (Cases 5 and 6), Re_l decreases over part of the run. Turbulence intensity u' increases late in Case 4, presumably because of imperfect turbulence inlet boundary conditions. The microscale l_η increases with time. The lowest Reynolds number run is Case 5: there the integral scale is smaller than the laminar flame thickness and the turbulence intensity is of the order of the laminar flame speed. At the other extreme is Case 4 where $u'/s_l^0 \approx 7$–8 and $l/\delta_{ll} > 10$ at later times. The largest value of the ratio l_η/δ_{ll} is for Case 8 ($l_\eta/\delta_{ll} \approx 0.5$); for all other cases, the microscale l_η is a quarter to a third of the undisturbed laminar flame thickness.

In the classic picture, the ratios of scales for all cases reported here places these flames in the transition between 'thick' and 'thin' flames distinguished, loosely, by the criterion $l_\eta/\delta_{ll} = 1$ (Williams 1985). We are thus far from the limit of an infinitesimally thin flame sheet separating reactants from products. The overlap of chemical scales and turbulence scales complicates the analysis but perhaps renders the results more typical of practical turbulent flames (see §5).

The range of scales of turbulent motions that can influence the local flame structure has been debated widely. Recent numerical simulations by Poinsot *et al.* (1991) suggest that the smallest scales of motion cannot influence the flame structure because motions on the scale of l_η or l_k lack sufficient energy. This issue is not

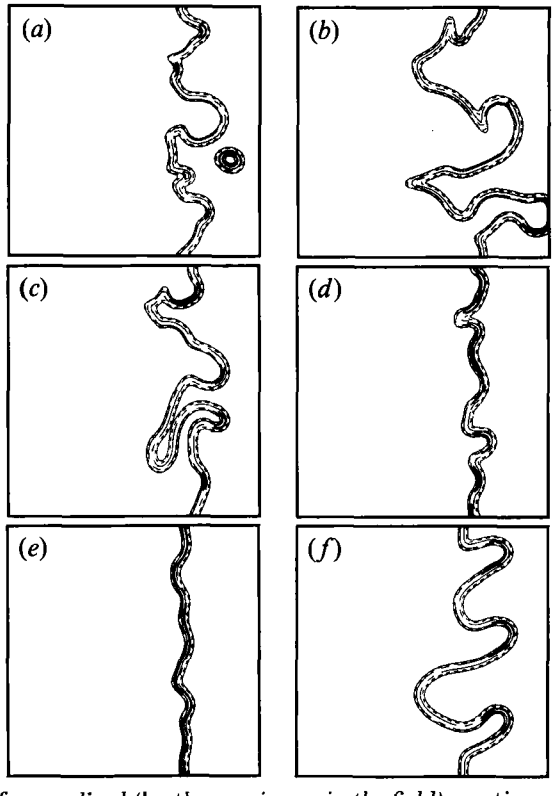

FIGURE 4. Examples of normalized (by the maximum in the field) reaction rate contours for several flames. Isocontours 0.015, 0.05, 0.25, and 0.6 are plotted: (*a*) Case 4*b*; (*b*) Case 4*d*; (*c*) Case 3*b*; (*d*) Case 6*c*; (*e*) Case 5*c*; (*f*) Case 8*c*.

addressed here directly. We do adopt a laminar flamelet approach in our diagnostics and discussion of these flames. It will be clear, we believe, that this is the most appropriate framework in which to discuss the results.

Typical contours of reaction rate for several flames are shown in figure 4. These illustrate the variety of flame behaviour that results from the differences in parameter ranges seen in tables 1 and 4. For the highest turbulence intensity (Case 4 at early times), islands of reactants are formed (figure 4*a*). These must eventually burn out for these adiabatic flames since there is no mechanism for extinction. The same flame at a much later time is shown in figure 4(*b*). There it can be seen that the initially planar flame now spans over half of the computational domain. The other four flames presented in figure 4 illustrate the effect of changing the initial turbulence lengthscale (figure 4(*c vs. d*)) and the initial turbulence intensity (figure 4(*d vs. e*)) while all other parameters remain fixed. The smaller lengthscale of figure 4(*d*) compared 4(*c*) yields a flame with less large-scale wrinkling while the smaller turbulence intensity of figure 4(*e*) compared to figure 4(*d*) results in a flame that is only mildly perturbed from the undisturbed planar laminar flame. Figure 4(*c*) represents one of the three flames that will be analysed in detail in the following section (Case 3*b*). Figure 4 (*f*) shows a flame with low u' and large l: in this case, there is large-scale folding but no fine-scale wrinkling.

3.3. *Diagnostics*

Postprocessing of the two-dimensional computed fields (snapshots at fixed times) begins by defining a flame front as an isocontour of either reduced temperature Θ or of normalized reactant mass fraction $\tilde{Y}$. Unless otherwise specified, the $\tilde{Y} = 0.3$ isocontour has been used to define the flame in the results that follow; this contour lies slightly in front of the reaction zone towards the fresh gases.

Once the flame has been located, the local normal n (equation (A 16)), local flame curvature $\mathscr{R}^{-1}$ (equation (A 15)), and local hydrodynamic strain rates normal to and tangent to the flame a_n and a_t (equation (A 17)) are readily computed. Curvatures concave towards the hot products are taken to be positive. Details can be found in the Appendix §A 2. Because the present computations include dilatation effects, it is important to distinguish between the tangential and the normal strain rates: the tangential component is used here for purposes of correlating the local flame structure since the normal component is dominated by the volume expansion through the flame. Sensitivity studies show no systematic dependence of the calculated distribution of tangential strain rates and curvatures to choice of flame isocontour in the range $0.2 \leqslant \tilde{Y} \leqslant 0.6$ for our runs. The normal strain rate, on the other hand, is extremely sensitive to this choice.

To compile statistics of the local structure of the turbulent flame, a set of one-dimensional profiles normal to the flame are taken. Typically 500–1000 profiles are obtained along the contour defining the flame. We compare these local turbulent flame profiles with the steady one-dimensional laminar flame profile for the same chemical and fluid properties. Of particular interest is the distribution along the flame of the normalized local flamelet speed s_l^* of equation (5).

The total flame area (length in two dimensions) and area-weighted (arclength-weighted) statistics of s^*, $\mathscr{R}^{-1}$, a_t, and a_n are calculated. The mean consumption rate of reactants per unit area of flame surface ('mean flamelet speed'), normalized by the laminar flame value, is computed as,

$$\langle s_l^* \rangle = \langle s_l / s_l^0 \rangle = \int_{L_{\text{flame}}} s_l^* \, \mathrm{d}l / L_{\text{flame}} = \int_{L_{\text{flame}}} s_l \, \mathrm{d}l / (s_l^0 L_{\text{flame}}), \tag{15}$$

where L_{flame} is the flame length. The global fuel consumption rate is calculated as the area integral of the reaction rate term in (10). This is related to the mean flamelet speed $\langle s_l \rangle$ and flame surface-to-volume ratio Σ (length-to-area ratio in two dimensions) as follows:

$$\begin{aligned} \overline{\dot{w}} &= \int_S \dot{w} \, \mathrm{d}\sigma / S = \int_{L_{\text{flame}}} \left(\int \dot{w} \, \mathrm{d}n \right) \mathrm{d}l / S \\ &= \int_{L_{\text{flame}}} \rho_1 s_l \, \mathrm{d}l / S = \rho_1 \langle s_l \rangle L_{\text{flame}} / S = \rho_1 \langle s_l \rangle \Sigma, \end{aligned} \tag{16}$$

where S is the total area of the computational domain. A normalized flame length $\mathscr{L}^*$ and turbulent flame speed s_T^* are defined as,

$$\mathscr{L}^* \equiv \Sigma / \Sigma_0 = L_{\text{flame}} / L_{\text{flame}0}, \tag{17}$$

$$s_T^* \equiv \overline{\dot{w}} / \overline{\dot{w}_0} = \langle s_l^* \rangle \mathscr{L}^*, \tag{18}$$

where the subscript '0' refers to the value at time $t = 0$ for the initially planar flame. A check of self consistency of the diagnostics is to verify the equality between s_T^*

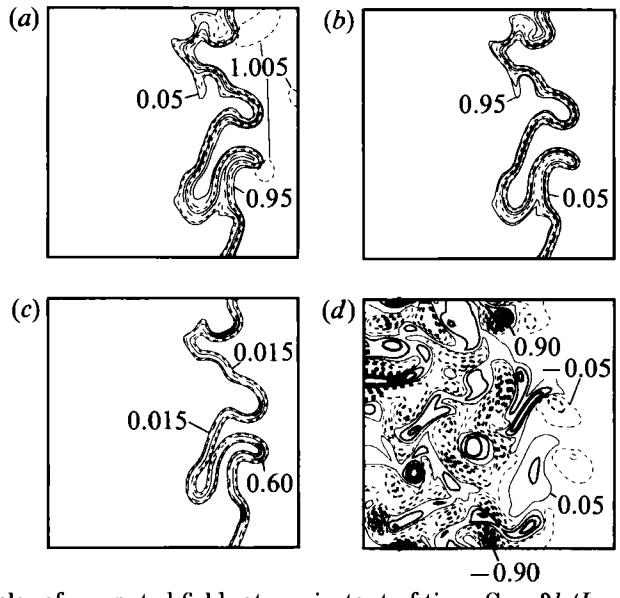

FIGURE 5. Examples of computed fields at one instant of time, Case 3*b* ($Le = 1.2$, $t/\tau_0 = 1.96$): (*a*) normalized temperature Θ (= 0.05, 0.1, 0.3, 0.5, 0.7, 0.9, 0.95, 1.005); (*b*) normalized reactant mass fraction $\tilde{Y}$ (= 0.05, 0.1, 0.3, 0.5, 0.7, 0.9, 0.95); (*c*) normalized reaction rate $\dot{w}/\dot{w}_{\max}$ (= 0.015, 0.05, 0.25, 0.6); (*d*) normalized vorticity $\Omega/|\Omega_{\max}|$(= ±0.05, ±0.22, ±0.39, ±0.56, ±0.73, ±0.9; ——, $\Omega > 0$, – – –, $\Omega < 0$).

calculated as $s_T^* = \int_S \dot{w}\,d\sigma/(\int_S \dot{w}\,d\sigma)_0$ versus $s_T^* = \langle s_I^* \rangle \mathscr{L}^*$: these are found to agree to within a few per cent in all cases.

Typical fields of temperature, reactant mass fraction, reaction rate, and vorticity are shown in figure 5 (Case 3*b*). There it can be seen (as in figure 4) that the initially planar flame has been strongly deformed by the turbulence. The suppression of post-flame velocity fluctuations by viscosity is evident. Another point that can be made is that for this non-unity Lewis number case, differential diffusion of heat versus species results in mass fractions and temperature that are not simply related by $\Theta + \tilde{Y} = 1$. In particular, temperatures behind the flame for the $Le = 1.2$ flames exceed the adiabatic flame temperature: there is a pocket of $\Theta > 1$ behind each of the concave-towards-reactants folds.

4. Results

Results for $Le = 0.8$, 1.0 and 1.2 flames are reported, concentrating on the Cases 1*b*, 2*b* and 3*b* of table 1. We begin with presentation and discussion of statistics of flame front curvature and strain rates. Next, the local structure of the turbulent flame is described; the local flame structure is compared with that of an undisturbed planar laminar flame at the same Lewis number. Finally, global quantities of interest in the description of turbulent premixed flames (flame surface, mean consumption rate per unit area of flame, and turbulent flame speed) are given. Further discussion of the results can be found in §5.

4.1. *Statistics of flame curvature and strain rate*

Typical p.d.f.s of flame curvature (normalized by the undisturbed laminar flame thickness δ_{l1}) are shown in figure 6. It may be seen that the p.d.f.s are close to symmetric with mean values near zero and with few curvatures exceeding the

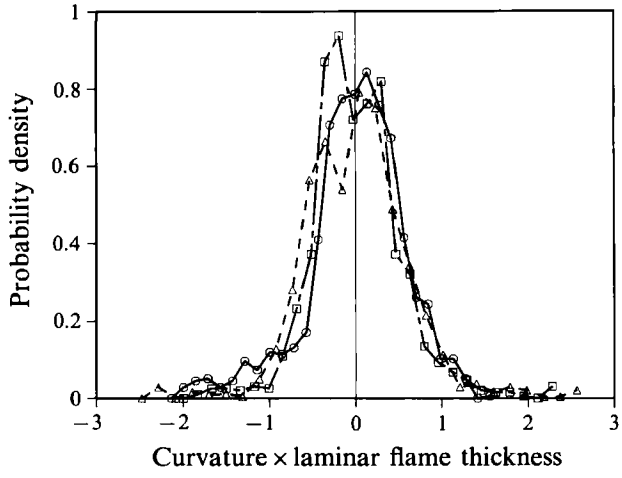

FIGURE 6. P.d.f.s of flame curvature $\mathscr{R}^{-1}$ normalized by the undisturbed laminar flame thickness δ_{l1} for the same Lewis number: ○, Case 1*b*, $Le = 0.8$; △, Case 2*b*, $Le = 1.0$; □, Case 3*b*, $Le = 1.2$.

reciprocal of the laminar flame thickness. The smallest radii of curvature are equal to about $\frac{1}{2}\delta_{l1}$, consistent with results obtained by Poinsot *et al.* (1992) in a study of Bunsen burner flame tips. Although the most probable curvature is higher for $Le = 0.8$ than for $Le = 1.2$ for the particular case shown in figure 6, this is not statistically significant: no systematic dependence on Lewis number is found. Curvature p.d.f.s for all runs at all times share these features. However, it must be pointed out that all Lewis numbers used in this study are above the critical Lewis number. Values of Le less than $Le_c \approx 0.385$ might lead to different conclusions.

Tabulated mean and r.m.s. curvatures (normalized by δ_{l1}) are reported in table 3. There does appear to be a weak systematic bias towards negative curvatures (concave towards the reactants) in the mean values; the maximum mean curvature magnitude for any run is $\langle \mathscr{R}^{-1} \rangle \cdot \delta_{l1} \approx -0.1$ for Case 1 at $t/\tau_0 = 1.94$ (not shown in table 4). The r.m.s. radii of curvature are of the order of one to two flame thicknesses. Significant asymmetry in the flame curvature p.d.f.s was fund in the three-dimensional computations of Rutland & Trouvé (1990*b*), which were performed for smaller values of u'/s_l^0 and constant density. Curvature p.d.f.s are expected to become more symmetric with increasing u'/s_l^0 (Becker *et al.* 1990; Bray 1990); such a trend is not evident in the present simulations.

One important difference between surfaces propagating with constant speed (e.g. Girimaji & Pope 1992) and flames is in the evolution of curvature. A flame must consume reactants to propagate, and regions of a flame that are strongly curved towards the reactants will not continue to propagate with constant speed to form a cusp (infinite curvature): minimum radii of curvature are limited to values that are of the order of (but smaller than) the laminar flame thickness. Thus the strong bias towards negative curvatures (in the present sign convention) seen in the simulations of Girimaji & Pope (1992) is not apparent in the present calculations.

P.d.f.s of tangential strain rate are given in figure 7. There it can be seen that positive strain rates are dominant – that is, the flame aligns preferentially with extensive strains. While the p.d.f.s again are noisy, examination of results for all cases computed reveals no apparent systematic dependence on Le. The dominance of extensive strain rates is also seen in three-dimensional simulations (Ashurst 1990; Girimaji & Pope 1992; El Tahry *et al.* 1991; Cant *et al.* 1990*b*; Rutland *et al.* 1990).

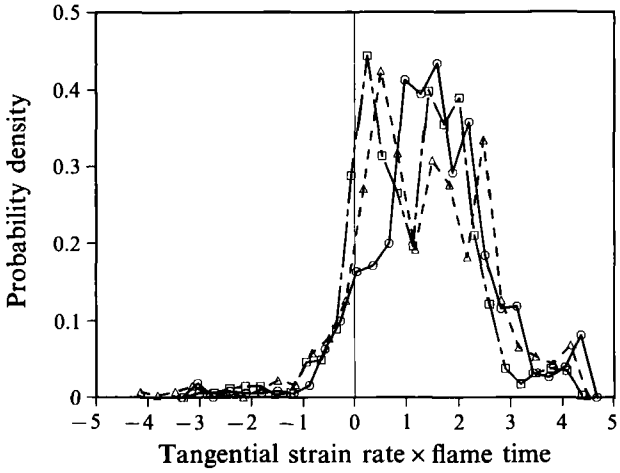

FIGURE 7. P.d.f.s of flame tangential strain rate a_t normalized by the chemical time τ_f for the same Lewis number: ○, Case 1*b*, $Le = 0.8$; △, Case 2*b*, $Le = 1.0$; □, Case 3*b*, $Le = 1.2$.

A strain Karlovitz number Ka_{st} is introduced to reflect the importance of turbulent straining:

$$Ka_{st} = \langle a_t \rangle \cdot \tau_f, \tag{19}$$

where $\langle a_t \rangle$ is the area-weighted tangential strain rate on the flame. Values of Ka_{st} for the various runs have been tabulated in table 3. It can be seen that, following an initial abrupt increase from zero,† the strain Karlovitz number tends to decrease with time. Values range from 0.2 to about 2 with the lowest values for Case 5 and the highest for Case 4. For the three cases that we are focusing on here (Cases 1*b*, 2b and 3*b*), $Ka_{st} > 1$.

The tangential strain rate in figure 7 and equation (19) has been scaled with the chemical time τ_f to emphasize interactions between chemistry and turbulence. If instead, we scale the mean tangential strain rate with the enstrophy micro-timescale τ_η as,

$$\langle a_t \rangle = C_\eta / \tau_\eta, \tag{20}$$

then it is found that the value of C_η various from zero at the beginning of the computations to a more or less steady value of 0.20–0.70 (table 3). We can also scale the mean tangential strain rate with the Kolmogorov timescale τ_k,

$$\langle a_t \rangle = C_k / \tau_k. \tag{21}$$

In this case, values of C_k range from 0.15 to 0.30 once the flame has become sufficiently wrinkled ($t/\tau_0 > \approx 1$, table 3). In three-dimensional simulations of propagating surfaces in forced isotropic turbulence, C_k is found to depend on the propagation speed p: for $p/u_k = 1.0$, $C_k \approx 0.16$ (non-area-weighted statistics; Girimaji & Pope 1992). Yeung, Girimaji & Pope (1990) reported $C_k = 0.28$ for material surfaces (using area-weighted statistics) and this same value was found for flames (constant property surfaces) propagating in low-Reynolds-number decaying turbulence by Cant *et al.* (1990*b*). We again emphasize that τ_k is probably not a physically meaningful scale for two-dimensional turbulence; it is shown here only for comparison with three-dimensional results.

† For the initially planar flame, $\langle a_t \rangle = \int_{L_{flame}} (\partial u_2/\partial x_2)\, dl / L_{flame} = 0$ by virtue of the periodic boundary condition in x_2, even though the flame is strained locally. This points out a weakness of characterizing the strain by $\langle a_t \rangle$ alone.

Case	Le	t/τ_0	$\langle\mathscr{R}^{-1}\rangle\delta_{l1}$	$\mathscr{R}^{-1}_{rms}\delta_{l1}$	Ka_{st}	$\tau_f a_{t_{rms}}$	C_η	C_k	$\langle s_l^*\rangle$	s_T^*	$\mathscr{L}^*$	l_{brush}/l	$l_{\mathscr{R}}/\delta_{l1}$
1*a*	0.8	0.00	0.00	0.00	0.00	1.74	0.00	0.00	1.00	1.00	1.00	0.00	0.00
1*b*	0.8	1.95	−0.01	0.58	1.47	1.17	0.41	0.18	1.14	2.88	2.51	2.35	0.89
1*c*	0.8	2.92	−0.07	0.65	0.99	0.99	0.34	0.16	1.14	2.73	2.40	2.86	1.05
2*a*	1.0	0.00	0.00	0.00	0.00	2.04	0.00	0.00	1.00	1.00	1.00	0.00	0.00
2*b*	1.0	1.96	−0.02	0.73	1.25	1.31	0.38	0.17	1.01	2.50	2.53	2.26	1.00
2*c*	1.0	3.79	0.08	0.60	0.79	0.85	0.35	0.17	1.02	2.24	2.20	2.00	1.15
3*a*	1.2	0.00	0.00	0.00	0.00	1.72	0.00	0.00	1.00	1.00	1.00	0.00	0.00
3*b*	1.2	1.96	−0.02	0.60	1.09	1.09	0.39	0.18	0.86	2.02	2.38	2.21	1.11
3*c*	1.2	3.91	−0.03	0.58	0.69	0.78	0.37	0.18	0.88	1.84	2.18	1.90	1.14
4*a*	1.2	0.00	0.00	0.00	0.00	3.39	0.00	0.00	1.00	1.00	1.00	0.00	0.00
4*b*	1.2	2.53	−0.06	0.84	1.70	1.70	0.34	0.15	0.90	1.93	1.98	1.98	0.82
4*c*	1.2	4.85	−0.02	0.60	1.00	1.32	0.31	0.13	0.86	1.78	2.14	1.17	1.17
4*d*	1.2	7.76	−0.02	0.67	1.19	1.86	0.46	0.18	0.90	2.47	2.96	0.84	0.89
5*a*	1.2	0.00	0.00	0.00	0.00	0.93	0.00	0.00	1.00	1.00	1.00	0.00	0.00
5*b*	1.2	3.50	−0.02	0.60	0.39	0.78	0.17	0.12	0.97	1.02	1.07	5.46	1.15
5*c*	1.2	7.55	−0.04	0.46	0.19	0.46	0.15	0.11	0.98	1.03	1.06	4.38	1.58
6*a*	1.2	0.00	0.00	0.00	0.00	1.87	0.00	0.00	1.00	1.00	1.00	0.00	0.00
6*b*	1.2	2.78	0.00	0.81	1.01	1.44	0.25	0.14	0.93	1.07	1.19	3.53	0.88
6*c*	1.2	4.88	−0.02	0.69	0.86	1.02	0.31	0.18	0.95	1.21	1.29	3.86	1.12
6*d*	1.2	7.45	−0.02	0.65	0.57	0.76	0.29	0.17	0.94	1.19	1.28	3.14	1.18
7*a*	1.2	0.00	0.00	0.00	0.00	1.90	0.00	0.00	1.00	1.00	1.00	0.00	0.00
7*b*	1.2	1.22	−0.04	0.70	1.54	1.36	0.43	0.19	0.85	1.66	2.01	2.03	1.07
7*c*	1.2	2.44	−0.06	0.65	0.85	0.93	0.32	0.15	0.84	1.86	2.24	2.17	0.97
8*a*	1.2	0.00	0.00	0.00	0.00	0.39	0.00	0.00	1.00	1.00	1.00	0.00	0.00
8*b*	1.2	0.52	−0.02	0.54	0.72	0.55	0.73	0.31	0.90	1.41	1.57	1.20	1.40
8*c*	1.2	0.98	−0.03	0.52	0.63	0.64	0.73	0.32	0.89	1.91	2.16	1.54	1.37

TABLE 3. Flame statistics for all cases

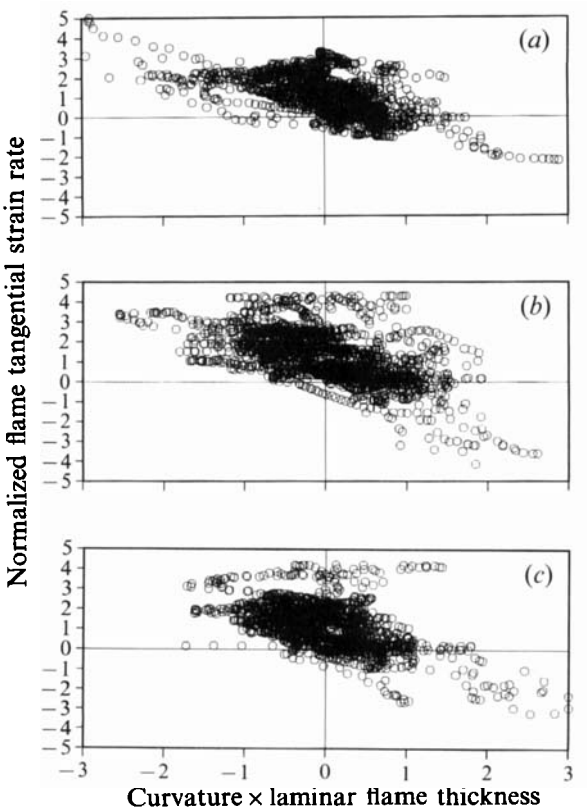

FIGURE 8. Scatter plots of normalized flame tangential strain rate $a_t\tau_f$ versus normalized flame curvature $\mathscr{R}^{-1}\delta_{ij}$: (*a*) Case 1*b*, $Le = 0.8$; (*b*) Case 2*b*, $Le = 1.0$; (*c*) Case 3*b*, $Le = 1.2$.

An important difference between the present results and those obtained for propagating surfaces (Girimaji & Pope 1992) is in the dependence of C_k on p/u_k (analogous to our s_1^0/u_η). In most of the present simulations, s_1^0/u_η is close to unity (table 4) and C_k and C_η remain more or less constant after $t/\tau_0 > 1$. The most extreme values are for Case 5 (low C_η and C_k) and Case 8 (high C_η and C_k), two runs with low initial u'/s_1^0. For propagating surfaces, Girimaji & Pope (1992) find that C_k decreases with increasing p/u_k while no clear trend is evident here.

Another interesting feature of the strain–curvature statistics is that in all cases, a strong correlation is found between local tangential strain rate and local flame curvature. This correlation is illustrated in figure 8 for Cases 1*b*, 2*b* and 3*b*; similar results are found in every case. Positive curvatures (concave towards products) correlate with negative (compressive) tangential strain rates and negative curvatures with extensive tangential strain rates. This is somewhat different from the results found for propagating surfaces (Girimaji & Pope 1992): there, highly curved regions correlated with compressive strain rates and less curved regions with extensive strain rates, especially at higher propagation speeds. It appears that the dominant mechanism producing high local tangential strain rates in the present simulations is a counter-rotating vortex pair: this structure tends to correlate curvature and strain rate in the manner seen in figure 8 (figure 1*d*). Although we believe that this curvature–strain rate correlation is a result of the asymmetry of the turbulence (high in the pre-flame gases, low in the post-flame region), we reckon that the specific

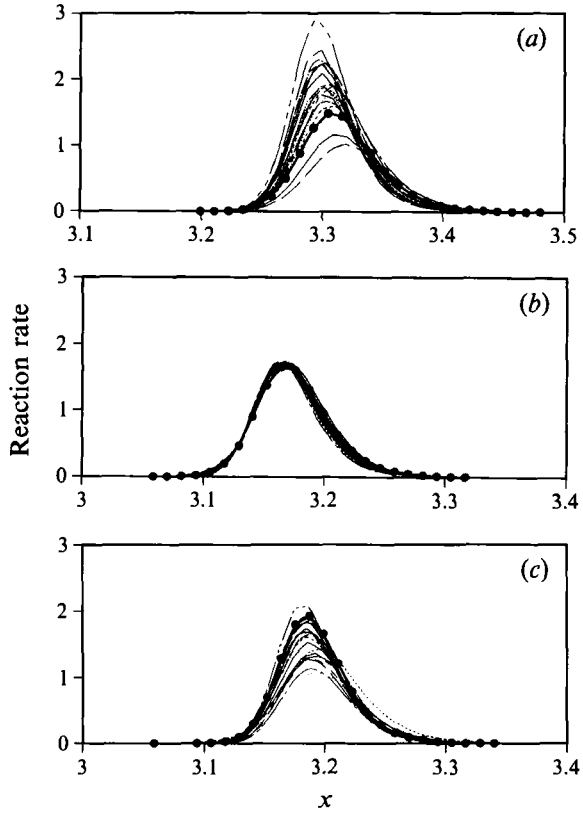

FIGURE 9. Local reaction rate profiles normal to the turbulent flame (lines) superposed on the steady undisturbed planar laminar flame reaction rate profile (symbols) for the same Lewis number. Profiles are sampled uniformly along the turbulent flame: (*a*) Case 1*b*, $Le = 0.8$; (*b*) Case 2*b*, $Le = 1.0$; (*c*) Case 3*b*, $Le = 1.2$.

features of the computation (two-dimensional, periodic boundary conditions in x_2) also might play a role; this result should be investigated in other geometries. Volume dilatation coupled with curvature may also be a factor. In this scatter plot and those that follow, samples are distributed uniformly in arc length along the flame. Thus the density of points in a specified region of each plot is proportional to the length (area) of flame having the values associated with that region.

A consequence of the correlation between tangential strain rate and curvature is that for both the $Le = 0.8$ and the $Le = 1.2$ flames, strain and curvature influences on s_1^* tend to work in opposite directions. That is, for $Le = 0.8$, extensive tangential strains which tend to increase s_1^* occur more frequently with negative (concave towards reactants) curvatures which tend to decrease s_1^*. And, for $Le = 1.2$, extensive tangential strains which decrease s_1^* correlate with curvatures concave towards the reactants which speed up the flame.

4.2. *Local flame structure*

The local flame structure, as illustrated through one-dimensional profiles of reaction rate, is shown in figure 9 for each of the three Lewis numbers simulated. There it is clear that the local flame structure is everywhere nearly identical to that of an undisturbed laminar flame for $Le = 1$ (figure 9*b*) while for non-unity Lewis numbers, there is no collapse of the local turbulent flame profiles onto the one-dimensional

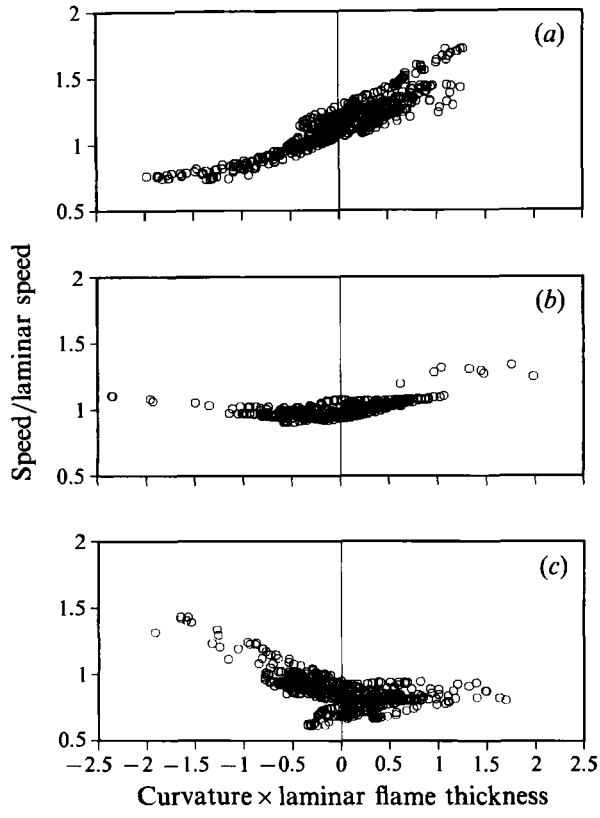

FIGURE 10. Scatter plots of normalized local flamelet speed s_l^* versus normalized local flame curvature $\mathscr{R}^{-1}\delta_{l1}$: (*a*) Case 1*b*, $Le = 0.8$; (*b*) Case 2*b*, $Le = 1.0$; (*c*) Case 3*b*, $Le = 1.2$.

undisturbed laminar flame profile (figure 9*a*, *c*). The $Le = 0.8$ reaction rate profiles tend to lie above the undisturbed laminar flame profiles (at the same Lewis number) while the $Le = 1.2$ profiles generally are lower than the corresponding laminar profile. This general trend is compatible with the dominant extensive strain rates which decrease s_l^* for $Le > 1$ and increase s_l^* for $Le < 1$.

From the discussion of thermodiffusive effects given earlier, we expect to see a correlation between local flame curvature and the local flamelet speed; indeed, this is the case. Figure 10 illustrates this correlation for each of the three Lewis numbers computed. For $Le = 0.8$ (figure 10*a*), flame elements concave towards reactants tend to have lower local flamelet speed and conversely for elements concave towards products; for $Le = 1.0$ (figure 10*b*), there is at most a weak correlation between local curvature and local flame structure; and, for $Le = 1.2$ (figure 10*c*), the correlation is opposite to that shown in figure 10*a*. Similar correlations between s_l^* and $\mathscr{R}^{-1}$ are observed in most of the Cases tabulated in table 4 for $t/\tau_0 > 0$. The numerical evaluations of curvature and of the integral along the flame normal for s_l^* (equation (5)) are somewhat noisy, however; thus the correlation with $\mathscr{R}$ of the maximum reaction rate along the flame normal tends to be clearer than the correlation of s_l^*. The $Le = 1.2$ scatter plots generally show a weaker correlation for $\mathscr{R} > 0$ than for $\mathscr{R} < 0$ (figure 10*c*).

Since $Ka_{st} > 1$ for the three runs that we are concentrating on, we might expect to see a correlation between local flamelet speed and local tangential strain rate. When

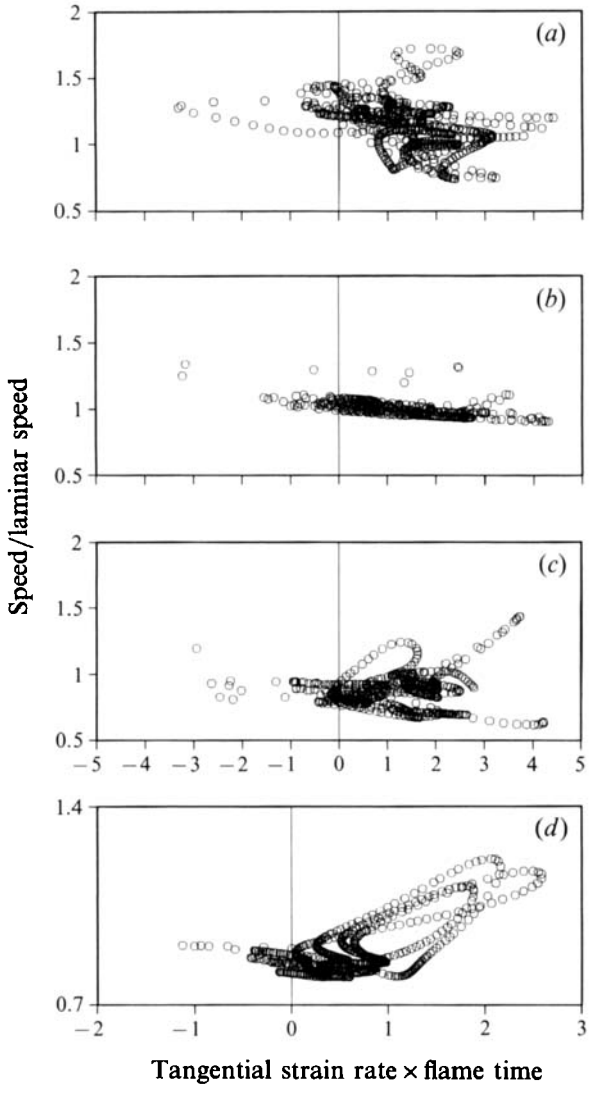

FIGURE 11. Scatter plots of normalized local flamelet speed s_l^* versus normalized local flame tangential strain rate $a_t \tau_f$: (*a*) Case 1*b*, $Le = 0.8$; (*b*) Case 2*b*, $Le = 1.0$; (*c*) Case 3*b*, $Le = 1.2$; (*d*) Case 8*c*, $Le = 1.2$.

the data are plotted in this way, the scatter plots of figure 11 result. There is no apparent systematic correlation evident for the non-unity Lewis number case of table 1; for $Le = 1.0$, a small negative slope can be seen in figure 11 (*b*), consistent with our expectation that extensive strains will slow the $Le = 1$ flame. In fact, for low Ka_{st} cases, the correlation of s_l^* with local tangential strain rate can be opposite to the expected trend for a planar laminar flame (figure 11*d*). This is a result of the strong curvature-strain rate correlation and the opposing influences of $\mathscr{R}^{-1}$ and a_t on s_l^*.

That the correlation of s_l^* with $\mathscr{R}^{-1}$ tends to be stronger than the correlation of s_l^* with a_t implies that curvature plays the dominant role in determining the local flame structure for non-unity Lewis numbers, at least over the parameter ranges calculated here. This occurs in spite of the fact that $Ka_{st} > 1$ for most of these runs and in spite

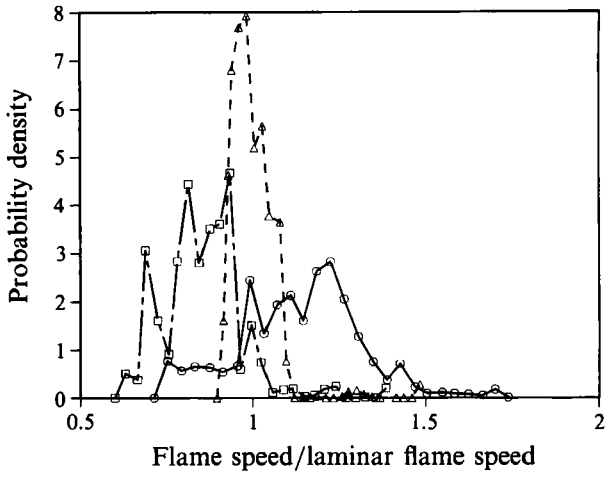

FIGURE 12. P.d.f.s of normalized local flamelet speed s_l^*: ○, Case 1*b*, $Le = 0.8$; △, Case 2*b*, $Le = 1.0$; □, Case 3*b*, $Le = 1.2$.

of the counterbalancing effect of the curvature–strain rate correlation seen in figure 8. This does not mean that turbulent straining is not important: evidence to the contrary is presented in the following subsection.

4.3. *Global quantities*

The mean reaction rate along the turbulent flame (mean flamelet speed) and the flame surface area are quantities of interest in constructing flamelet models for turbulent premixed combustion. In figure 12, examples of p.d.f.s of the normalized local flamelet speed in the turbulent flame are shown for each of the three Lewis numbers. For non-unity Lewis numbers, it can be seen that the p.d.f. of flamelet speed is broadened and shifted relative to $Le = 1.0$. The unity Lewis number case shows only a small spread about the undisturbed laminar flame speed. The area-averaged normalized mean flamelet speeds $\langle s_l^* \rangle$ for the three cases shown in figure 12 are 1.14 ($Le = 0.8$); 1.00 ($Le = 1.0$); and 0.86 ($Le = 1.2$). Table 3 reports $\langle s_l^* \rangle$ for all runs. There it can be seen that $\langle s_l^* \rangle$ remains close to unity for the low Re_l, $Le = 1.2$ runs of Cases 5 and 6.

As mentioned earlier, the density of points in the scatter plots of figures 10 and 11 is proportional to the area of flame in each region of the plots. If we model the scatter plots of figure 10 as being linear ($s_l^* = m\mathscr{R}^{-1} + b$; $m \approx 0.3$ and $b \approx 1.2$ for figure 10*a* in the normalized units plotted there; $m \approx -0.3$ and $b \approx 0.8$ for figure 10*c*) and model the curvature p.d.f.s of figure 6 as being symmetric with zero mean, then curvature would have no influence on $\langle s_l^* \rangle$ and straining effects can become apparent. The shifting of $\langle s_l^* \rangle$ to values greater than unity for $Le < 1.0$ and to values less than unity for $Le > 1.0$ is consistent with the positive mean tangential strain rate $\langle a_t \rangle$ seen in figure 7 and table 3. Thus while curvature is dominant in influencing the local flame structure, the global consumption rate per unit area of flame $\langle s_l^* \rangle$ appears to be dominated by the mean tangential strain rate.

For propagating surfaces (Girimaji & Pope 1992), it has been found that the strain rate following a propagating surface element is sustained for times of the order of the turbulence micro-timescale τ_k. Curvature of a flame element can be expected to be sustained longer for $\mathscr{R} < 0$ than for $\mathscr{R} > 0$ because self-propagation amplifies negative curvature but reduces positive curvature. Moreover, the thermodiffusive

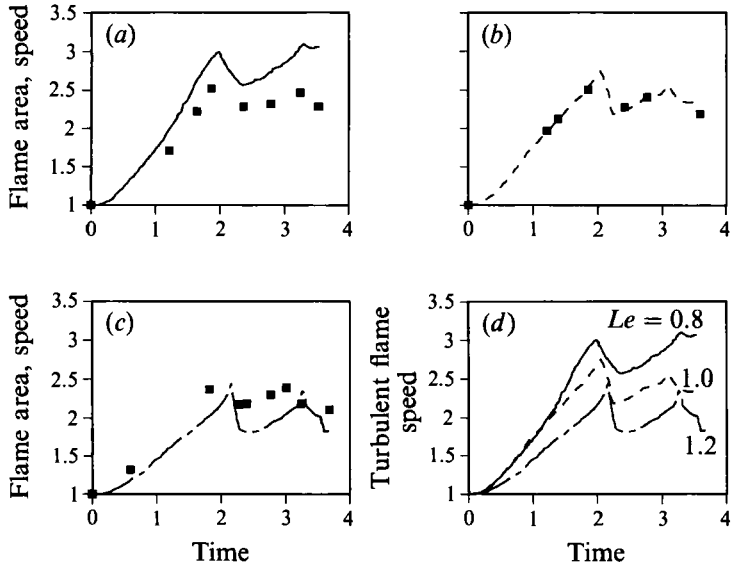

FIGURE 13. Evolution with normalized time t/τ_0 of normalized turbulent flame speed s_T^*(lines) and flame length $\mathscr{L}^*$ (symbols): (*a*) Case 1*b*, $Le = 0.8$; (*b*) Case 2*b*, $Le = 1.0$; (*c*) Case 3*b*, $Le = 1.2$; (*d*) s_T^* versus t/τ_0 for three Lewis numbers.

effect is expected to sustain flame curvature for $Le < 1$ (departures from planar amplified) longer than for $Le > 1$ (departures from planar damped). Thus there are mechanisms by which we can expect flame curvature to be relatively more important for $\mathscr{R} < 0$ than for $\mathscr{R} > 0$, and more important for $Le < 1$ than for $Le > 1$. The results of figure 10 are consistent with this: there it appears that curvature is dominant for $Le < 1$ for both positive and negative curvatures (figure 10*a*) while for $Le > 1$, turbulent straining is able to weaken the otherwise strong correlation of s_l^* with $\mathscr{R}$ for $\mathscr{R} > 0$ (figure 10*c*).

Figure 13 illustrates the Lewis number effects in a different way. There the variation with time of the normalized turbulent flame speed s_T^* (equation (18)) and normalized flame length $\mathscr{L}^*$ (equation (17)) are plotted as functions of time for Cases 1, 2 and 3. The turbulent flame speed is (normalizations aside) the product of the mean flamelet speed and the flame length. The interesting finding is that the turbulent flame speed increases more rapidly than the flame area for $Le = 0.8$; that for $Le = 1.0$, these two quantities evolve identically; and, that for $Le = 1.2$, the flame surface increase exceeds the turbulent flame speed augmentation. Figure 13(*d*) repeats the turbulent flame speed curves for the three Lewis numbers to emphasize the decrease in turbulent flame speed with increasing Lewis number.

We have already seen one mechanism for the strong Lewis number dependence of s_T^*, namely, the increase in the mean consumption rate per unit flame area $\langle s_l^* \rangle$ for $Le < 1$ and conversely for $Le > 1$. A secondary cause is that (slightly) more flame area is generated for $Le = 0.8$ than for $Le = 1.2$. The difference is small, about 5–10%, for the cases shown in figure 13. This effect presumably would be more pronounced under thermodiffusively unstable conditions ($Le < Le_c$): recall that $Le > Le_c$ in the present calculations. Similarly, one might expect to see a broadening or increased variance in the curvature p.d.f.s for $Le < Le_c$.

Another global aspect of the flame structure that is of interest is the scales of wrinkling. Two simple scales have been introduced in equations (A 18) and (A 19).

There l_{brush} (width of turbulent flame brush) is a length characteristic of the largest scales of wrinkling and $l_{\mathscr{R}}$ (a curvature-based scale) is characteristic of the smallest. These values (suitably normalized) are reported in table 3. There it can be seen that with the exception of low-Reynolds-number Cases 5 and 6, l_{brush} generally ranges from one to two times the turbulence integral lengthscale l while $l_{\mathscr{R}}$ is of the order of the laminar flame thickness.

5. Discussion

Most numerical simulations and phenomenological models of turbulent premixed combustion have not included nonunity Lewis number effects (Bray & Libby 1986; Candel *et al.* 1988; Pope & Cheng 1988; Cant & Bray 1988; Maistret *et al.* 1989; El Tahry 1990; Cant *et al.* 1990*a*; Bray 1990). The present results suggest that in fact, the Lewis number has a strong influence on the local and global structure of turbulent flames. While straining has been shown to have an influence on the distribution of local flamelet speed in $Le = 1$ flames, this effect is small compared to the large strain and curvature effects on both local and global quantities that have been found in the non-unity Lewis number simulations.

Complex chemistry of hydrocarbon fuels makes the definition of a single mixture Lewis number problematic: a Lewis number can be defined for each species and these Lewis numbers will be spatially non-uniform. Hydrogen, for example, diffuses in air at about twice the rate of a light hydrocarbon such as methane. Away from stoichiometric, the most relevant Lewis number influencing overall reactant consumption rate reasonably can be expected to be the Lewis number based on diffusion of the limiting (deficient) reactant through the pre-heat zone and into the reaction zone (Williams, private communication). Hence the results reported here for single-step chemistry and uniform Lewis number may remain qualitatively valid for more complex kinetics.

An overall Lewis number based on the deficient reactant can be calculated using a complex-chemistry stagnation-point flame code. Adopting this approach, Blint (private communication) has found that Lewis numbers for methane–air flames for equivalence ratios of 0.8 to 1.2 are well within the range of $0.8 \leqslant Le \leqslant 1.2$ covered in the present study ($Le < 1$ for fuel-lean). Methane is not typical of heavy hydrocarbon fuels, however. Moreover, the deficient-reactant-based Lewis number is inadequate close to stoichiometric. For example, fuel-based Lewis numbers for propane–air flames range from 1.7 to 1.9 for equivalence ratios between 0.3 and 2.0, while Lewis numbers based on oxygen or nitrogen remain close to unity over this range of equivalence ratios. (These values have been computed for atmospheric pressure flames with $T_1 = 300$ K; Blint, private communication.) This implies a step change in Lewis number at stoichiometric that is not physically meaningful: a single global Lewis number based on deficient reactant does not suffice close to stoichiometric (Chelliah & Williams 1987; Williams, private communication). In general, Lewis numbers are greater than unity for heavy hydrocarbon fuels at lean conditions typical of internal combustion engine operation. This may contribute to the 'robustness' of the wrinkled flame sheet combustion regime in engines.

Experimental validations of the present computational results require local instantaneous measurements of the reaction rate in a turbulent flame, and thus constitute a practically challenging problem. However, qualitative support can be found in a number of recent experimental studies. Becker *et al.* (1990) have studied the influence of Lewis number on premixed turbulent flame structure using OH

fluorescence as a marker of the reaction zone. They observe a correlation between local burning rate (OH fluorescence intensity) and local flame curvature that is similar to that seen in the present $Le > 1$ computations. (The Lewis number based on fuel is greater than unity for their fuel-lean propane–air flame.) In the mean, curvature effects were found to be negligible for intense turbulence while remaining important for weak turbulence.

Additional corroborative evidence for strong Lewis number effects in high Reynolds number turbulent premixed flames may be found in the experiments of Wu *et al.* (1990), Cheng, Goix & Shepherd (private communication) and Lee, North & Santavicca (1991). In the former, substantial changes in flame wrinkling and flame length with changes in equivalence ratio for a premixed hydrogen–air jet flame are attributed to differential diffusion effects: for the same mean flow, turbulence intensity, and undisturbed laminar flame speed, Wu *et al.* (1990) report higher wrinkling and shorter flame length (implying larger reacting flame sheet area) by a factor of two for their fuel-lean flame ($Le < 1$) compared to their fuel-rich flame ($Le > 1$). Cheng *et al.* (private communication) find increased flame area and a higher fractal dimension, implying more fine-scale flame wrinkling, for $Le < 1$ than for $Le > 1$ in stagnation-point turbulent premixed flames for various fuel–air mixtures (for the same turbulence intensity and laminar flame speed). Lee *et al.* (1991) show symmetric flame curvature p.d.f.s having zero mean and variances that increase with increasing turbulence intensity and that are higher for $Le < 1$ than for $Le > 1$: these results are for freely propagating nearly one-dimensional flames at turbulence Reynolds numbers between 100 and 700.

Several qualitative similarities between present results and three-dimensional constant-density simulations have been pointed out, including the predominance of positive tangential strain rates and the scaling of $\langle a_t \rangle$ with turbulence microscales. Lewis-number effects in three-dimensional constant-property turbulence are the focus of the computational study by Rutland & Trouvé (1990). Differences between the present results and conclusions drawn from propagating surface simulations (Girimaji & Pope 1992) include the near symmetry of the flame curvature p.d.f.s, numerical values of C_k, and the strain rate–curvature correlation found in the present study.

Intentionally, we have not ventured to draw quantitative correlations from these results because of the two-dimensional, non-stationary (in a statistical sense) nature of the computations. Nevertheless, we feel that these calculations shed new light on the structure of turbulent flames, particularly in pointing out the importance of flame curvature and molecular effects on turbulent flame structure. Results of three-dimensional constant property simulations at parameter ranges far from those of practical flames are also likely to be quantitatively non-representative of high-Reynolds- and high Damköhler-number turbulent flames. The predominantly two-dimensional flame structure that has been found consistently in a number of three-dimensional computational studies of turbulent premixed flames or propagating surfaces (Ashurst 1990; Cant *et al.* 1990*b*; Girimaji & Pope 1992) lends support to the two-dimensional computational approach adopted here. Ashurst (1990) suggests that an improved two-dimensional representation would include a weak out-of-plane extensive strain to counteract (through vortex stretching) the viscosity-induced vorticity suppression through the flame that characterizes the present computations (figure 5*d*).

The results of this study have been explained in terms of classic thermodiffusive effects for laminar premixed flames. The relevance of molecular effects in high-

Reynolds-number flames bears some consideration. There are two issues: first, can molecular effects remain important as the Reynolds number continues to increase; and secondly, are molecular effects important at Reynolds numbers of interest in practical applications? The answer to both questions appears to be affirmative. As long as there remains a local flamelet-like structure to the turbulent flame, it is feasible that molecular effects could remain important at any arbitrarily high Reynolds number. Parameter ranges characterizing the flamelet regime of turbulent premixed combustion are the subject of a recent numerical study by Poinsot *et al.* (1991). Experimental evidence for thermal-diffusive effects in high-Reynolds number premixed jet flames has been discussed earlier.

To address the second issue, the ratios of scales in these computations is not atypical of those encountered in at least one important application of turbulent premixed combustion, that of a homogeneous-charge reciprocating engine. The flamelet character of the flame front in internal combustion engines has been verified in a number of visualization experiments (e.g. Mantzaras, Felton & Bracco 1988; Ziegler *et al.* 1988). While there remains a great deal of uncertainty in scale estimates for practical engines (Abraham, Williams & Bracco 1985; Bracco 1988; Blint 1988, 1991), the following ranges have been estimated for propane–air mixtures in a model engine (Mantzaras *et al.* 1988; Blint 1988, 1991). For undiluted stoichiometric flames, u'/s_1^0 ranges from 0.5 to 4 as engine speed increases from 300 to 2400 r.p.m.; for leaner mixtures (s_1^0 decreasing) or higher engine speed (u' increasing), the relative turbulence intensity is even higher. The lengthscale ratio l/δ_{11} ranges from about 30 for a baseline condition (stoichiometric, $p = 5$ atm, $T_1 = 600$ K, undiluted) to as low as three for stoichiometric high T_1, low p, or high exhaust-gas-dilution flames. Flame thicknesses generally are wider than the turbulence microscale: l_k/δ_{11} is equal to about a third for the baseline flame at 300 r.p.m. engine speed, but δ_{11} can be an order of magnitude larger than l_k for exhaust-gas-diluted flames. Turbulence Reynolds numbers Re_1 (based on unburnt gas viscosity) range from about 300 to 1500 even at low engine speeds of 300 r.p.m. to 1200 r.p.m; these Re_1 are higher than most of the cases computed here, although Case 4 falls in this range at later times (table 4). The regime of combustion represented by the present computations thus approaches the mode of combustion in at least one (moderate Reynolds number) application. We emphasize that the value of Re_1 reported in tables 1 and 4 can vary by a factor of two, depending on the choice of lengthscale l.

The present results have implications for the implementation of flamelet models of turbulent premixed combustion. The prototype laminar configuration for which flamelet libraries have been generated generally is that of a one-dimensional laminar stagnation-point burner. This configuration accounts, in some sense, for the effect of tangential strain, but does not account for flame-front curvature. The present results show that for non-unity Lewis numbers, the local flame structure is more strongly influenced by the local flame curvature than by the local tangential strain rate. The net consumption rate of reactants per unit area of flame (mean flamelet speed), however, appears to be most strongly influenced by straining. Thus in the construction of flamelet libraries, it may suffice to include only strain effects if it is the net consumption rate that is of interest. Predictions of phenomena such as quenching or pollutant formation that may be dominated by local hot or cold spots in the flame front, on the other hand, require that curvature be accounted for. The weak dependence of total flame surface area on Lewis number that has been found may be more important at higher Reynolds numbers where there is a broader range of hydrodynamic scales that can influence the flame.

6. Summary

Calculations of premixed turbulent flame structure in two-dimensional turbulence have been reported, focusing on the influence of Lewis number on the local and global flame structure. These computations include dilatation and variable transport coefficients. It has been found that:

(i) The local flamelet speed in the $Le = 1$ flame is everywhere nearly identical to that of an undisturbed laminar flame.
(ii) For $Le \neq 1$, the local flamelet speed differs from that of the undisturbed laminar flame and correlates strongly with local flame curvature.
(iii) Curvature effects cancel out when the mean flamelet speed (averaged along the flame front) is computed. Only flame strain effects persist to result in a mean flamelet speed that is higher than the laminar value for $Le < 1$, is identical to the laminar value for $Le = 1$, and is lower than the laminar value for $Le > 1$.
(iv) Thermodiffusive effects result in slightly more flame surface for $Le < 1$ than for $Le > 1$. This, combined with the strong dependence of mean flamelet speed on Le, results in a strong dependence of turbulent flame speed on Le.
(v) P.d.f.s of flame curvature are nearly symmetric with a near-zero mean value; the maximum curvatures found are of the order of the reciprocal of the laminar flame thickness.
(vi) P.d.f.s of strain rate tangent to the flame are skewed towards positive (extensive) strains with a mean strain rate of the order of the inverse of the timescale of the smallest turbulent motions.

These results imply that, for the range of parameters investigated, curvature is more important than strain rate in determining the local flame structure. However, the mean consumption rate per unit area of flame (averaged along the flame front) appears to depend primarily on the net positive mean tangential strain rate. The turbulent flame speed, which is the product of the flame area and the mean consumption rate, is therefore influenced slightly by thermodiffusive effects (which modify the flame area) and strongly by the mean strain rate (which creates flame area and modifies the mean consumption rate). Both effects influence the turbulent flame speed in the same way so that it is strongly Lewis number dependent. Stronger flame area effects, in particular, are expected in cases where the Lewis number Le is less than the critical value of Le_c ($Le > Le_c$ in all cases reported here).

Questions remaining to be addressed include: further comparisons between two- and three-dimensional calculations to quantify the limitations and virtues of each; relative contributions of straining versus curvature to the total flame stretch $A^{-1}\,\mathrm{d}A/\mathrm{d}t$; and, quantitative correlations between global quantities such as turbulent flame speed, turbulent r.m.s. velocity, and Lewis number.

This research was performed during D.C.H.'s visit as a participant in the 1990 summer program of the Stanford University/NASA Ames Center for Turbulence Research (CTR). The authors thank the organizers of the summer program for the opportunity to work together and for providing a stimulating working environment. Discussions with colleagues in the CTR combustion group Drs A. Trouvé, C. J. Rutland, R. S. Cant and W. T. Ashurst are gratefully acknowledged. D.C.H. also thanks management at GM Research for the opportunity to participate in the CTR program and GM colleagues Drs S. H. Tahry, M. C. Drake and R. J. Blint for discussion of the results of this study and their implications. In particular, we thank

Dr R. J. Blint for performing the Lewis-number computations. Discussions with Professor S. B. Pope of Cornell University on aspects of propagating surface computations (Girimaji & Pope 1992) have been illuminating.

Appendix

Velocity, length, and time scales characterizing the hydrodynamic field and the chemistry are introduced. Three sets of scales are calculated: scales characteristic of the large-scale turbulent motions; turbulence microscales representing the smallest fluid motions; and, chemical scales based on an undisturbed steady planar laminar flame. In §A.2, some procedural details of extracting flame curvature, strain rates, and wrinkling scales from the computed fields are given.

A.1. *Scales*

We restrict our attention to two-dimensional turbulence with instantaneous velocity components $u_1 = u_1(x_1, x_2, t)$, $u_2 = u_2(x_1, x_2, t)$. An overbar denotes a volume (area) average over the flow field while angled brackets $\langle\ \rangle$ will be reserved for flame-area-(length-) weighted means. All turbulence scales are calculated as conditional averages in the fresh reactants ($\tilde{Y} > Y_{\text{thresh}}$, with $Y_{\text{thresh}} = 0.9$).

Scales characteristic of the energy-containing turbulent motions are computed as follows. A root-mean-square turbulence intensity u' is calculated as,

$$u'^2 = \tfrac{1}{2}\{\overline{u_1'^2} + \overline{u_2'^2}\} = \frac{1}{2}\left\{\int_V [(u_1 - \overline{u_1})^2 + (u_2 - \overline{u_2})^2]\,\mathrm{d}\tau/V\right\}. \tag{A 1}$$

Definition of an appropriate lengthscale is more difficult. For comparison with model results, a dissipation-based scale l_ϵ is used conventionally,

$$l_\epsilon = u'^3/\epsilon. \tag{A 2}$$

Here ϵ is the viscous dissipation rate of turbulence kinetic energy,

$$\epsilon = \overline{2\nu s_{ij} s_{ij}}, \tag{A 3}$$

and $s_{ij} = \frac{1}{2}(\partial u_i/\partial x_j + \partial u_j/\partial x_i)$ is the rate-of-strain tensor. For homogeneous turbulence, longitudinal integral scales l_{11} and l_{22} based on two-point velocity correlations are computed as,

$$\left.\begin{aligned} l_{11} &= \int_0^\infty [u_1(x_1, x_2, t) - \overline{u_1(t)}]\,[u_1(x_1 + s, x_2, t) - \overline{u_1(t)}]\,\mathrm{d}s/\overline{u_1'^2}, \\ l_{22} &= \int_0^\infty [u_2(x_1, x_2, t) - \overline{u_2(t)}]\,[u_2(x_1, x_2 + s, t) - \overline{u_2(t)}]\,\mathrm{d}s/\overline{u_2'^2}. \end{aligned}\right\} \tag{A 4}$$

In three-dimensional high-Reynolds-number isotropic equilibrium turbulence, ϵ can be interpreted as the rate of spectral energy transfer from large to small scales through the inertial subrange: the lengthscales then are related by $l_{11} = l_{22} = Cl_\epsilon$ where C is a constant whose value depends on the details of the energy spectrum. Typically $C \approx 0.4$–0.5 (with $u'^2 = \frac{2}{3}k$; Tennekes & Lumley 1972; Hinze 1975). In the present simulations, we find in general that $l_{11} = l_{22}$ to within a factor of two, that l_ϵ typically is several times larger than l_{11}, and that L_t (equation (14)) also is several times larger than l_{11} at $t = 0$ (table 4). Inequality of l_{11} and l_{22} is attributed to

Case	Le	u_p/s_l^0	L_t/δ_{11}	t/τ_0	u'/s_l^0	l_c/l_{11}	l_{22}/l_{11}	l/δ_{11}	Re_λ	τ/τ_t	u_η/s_l^0	l_η/δ_{11}	τ_η/τ_t	l_η/l_k	τ_η/τ_k
1*a*	0.8	6.60	4.27	0.00	6.44	5.14	1.27	2.44	77	0.38	1.07	0.19	0.18	1.63	2.43
1*b*	0.8	6.60	4.27	1.95	4.82	3.33	1.04	3.60	86	0.74	0.87	0.24	0.28	1.49	2.23
1*c*	0.8	6.60	4.27	2.92	4.30	2.56	0.35	4.27	90	0.79	0.77	0.27	0.35	1.46	2.14
2*a*	1.0	6.28	4.46	0.00	6.10	5.11	1.27	2.54	77	0.41	1.02	0.20	0.20	1.64	2.69
2*b*	1.0	6.28	4.46	1.96	4.68	3.38	1.05	4.00	91	0.86	0.82	0.25	0.30	1.48	2.20
2*c*	1.0	6.28	4.46	3.79	3.95	2.66	0.57	5.83	111	1.48	0.68	0.31	0.45	1.45	2.08
3*a*	1.2	5.84	4.82	0.00	5.68	5.05	1.25	2.74	76	0.48	0.94	0.22	0.23	1.64	2.68
3*b*	1.2	5.84	4.82	1.96	4.32	3.21	1.04	4.26	88	0.99	0.76	0.27	0.36	1.48	2.20
3*c*	1.2	5.84	4.82	3.91	3.59	2.63	0.57	6.28	109	1.75	0.62	0.33	0.54	1.43	2.06
4*a*	1.2	8.76	3.23	0.00	8.40	4.23	0.93	2.04	85	0.24	1.33	0.15	0.11	1.67	2.78
4*b*	1.2	8.76	3.23	2.53	6.53	4.30	0.54	4.20	132	0.64	1.01	0.20	0.20	1.52	2.32
4*c*	1.2	8.76	3.23	4.85	7.08	4.69	0.43	11.2	381	1.59	0.82	0.26	0.31	1.57	2.49
4*d*	1.2	8.76	3.23	7.76	7.66	9.61	1.48	20.5	732	2.69	0.75	0.29	0.38	1.58	2.53
5*a*	1.2	2.92	2.06	0.00	2.08	0.90	0.90	0.35	4	0.17	0.93	0.22	0.23	1.31	1.71
5*b*	1.2	2.92	2.06	3.50	1.18	0.78	1.56	0.33	2	0.28	0.69	0.30	0.43	1.18	1.39
5*c*	1.2	2.92	2.06	7.55	0.84	0.67	1.10	0.42	2	0.50	0.51	0.40	0.78	1.15	1.32
6*a*	1.2	5.84	2.06	0.00	4.17	1.79	0.90	0.70	14	0.17	1.18	0.17	0.15	1.47	2.15
6*b*	1.2	5.84	2.06	2.78	2.70	2.15	1.86	0.81	11	0.30	0.91	0.23	0.25	1.33	1.77
6*c*	1.2	5.84	2.06	4.88	2.31	2.12	1.14	1.08	12	0.47	0.76	0.27	0.36	1.32	1.74
6*d*	1.2	5.84	2.06	7.45	2.07	1.59	0.32	1.54	15	0.74	0.64	0.32	0.50	1.31	1.74
7*a*	1.2	6.43	4.82	0.00	6.25	5.56	1.25	3.02	93	0.48	0.98	0.21	0.21	1.66	2.77
7*b*	1.2	6.43	4.82	1.22	5.03	4.29	1.83	3.80	93	0.76	0.86	0.24	0.28	1.52	2.31
7*c*	1.2	6.43	4.82	2.44	4.50	3.12	0.51	5.43	117	1.20	0.74	0.28	0.38	1.48	2.20
8*a*	1.2	2.92	9.64	0.00	2.70	6.24	2.04	4.87	65	1.80	0.47	0.43	0.91	1.63	2.64
8*b*	1.2	2.92	9.64	0.52	2.50	3.82	0.69	6.06	74	2.42	0.45	0.46	1.01	1.52	2.32
8*c*	1.2	2.92	9.64	0.98	2.43	4.24	0.31	7.59	90	3.11	0.42	0.49	1.16	1.51	2.28

TABLE 4. Dimensionless parameters for all cases

imperfect turbulence inlet boundary conditions and to statistical error in estimating these scales; the latter is particularly high for large-length-scale cases at late times where there may be only one or two integral scales of fresh gases in the computational domain. While at first sight the two-point integral scales of (A 4) might be expected to more rigorously represent the energy-containing motions, in fact, l_ϵ is found to be better behaved computationally (Poinsot 1991). Thus we adopt the lengthscale l defined by,

$$l \equiv 0.42 l_\epsilon = 0.42 u'^3/\epsilon. \tag{A 5}$$

The coefficient 0.42 is derived for a three-dimensional von Kármán spectrum (Hinze 1975) and also is close to the value obtained for the standard $k-\epsilon$ model. A turbulence timescale τ is formed using u' and l as,

$$\tau = l/u', \tag{A 6}$$

and a turbulence Reynolds number Re_1 is defined as,

$$Re_1 = u' l/\nu. \tag{A 7}$$

Because of the wide range of lengthscales that might legitimately be adopted to characterize the large-scale turbulent motions, it is essential that one be precise regarding scaling conventions when comparing the present scales and Reynolds numbers with experimental or turbulence modelling results.

Because there is no mechanism for an inertial-range cascade of energy from large to small scales in two-dimensional turbulence, it is not appropriate to take the Kolmogorov scales (based on ϵ and the fluid viscosity ν) as the scales characteristic of the smallest turbulent motions. Instead, it has been argued (Herring *et al.* 1974; Lesieur 1987) that appropriate microscales for two-dimensional turbulence should be defined using the mean-square vorticity or enstrophy Ω and its viscous dissipation rate η:

$$\Omega = 0.5\overline{|\nabla \times \boldsymbol{u}|^2}, \tag{A 8}$$

$$\eta = \overline{\nu|\nabla \times (\nabla \times \boldsymbol{u})|^2}. \tag{A 9}$$

Enstrophy-based microscales l_η (length), τ_η (time), and u_η (velocity) are then given as,

$$l_\eta = (\nu^3/\eta)^{\frac{1}{6}}, \quad \tau_\eta = \eta^{-\frac{1}{3}}, \quad u_\eta = l_\eta/\tau_\eta. \tag{A 10}$$

Kolmogorov microscales l_k, τ_k, and u_k also are reported, primarily for comparison purposes. These are defined as,

$$l_\mathrm{k} = (\nu^3/\epsilon)^{\frac{1}{4}}, \quad \tau_\mathrm{k} = (\nu/\epsilon)^{\frac{1}{2}}, \quad u_\mathrm{k} = l_\mathrm{k}/\tau_\mathrm{k}. \tag{A 11}$$

Chemical scales are based on the structure of an undisturbed planar laminar flame. The undisturbed laminar flame speed s_l^0 is taken as the velocity scale, and a lengthscale $\delta_{\mathrm{l}1}$ is defined based on the temperature profile.

$$s_\mathrm{l}^0 = \int \dot{w}\, \mathrm{d}n/\rho_1, \tag{A 12}$$

$$\delta_{\mathrm{l}1} = (T_2 - T_1)/(\mathrm{d}T/\mathrm{d}n)_{\max}, \tag{A 13}$$

where n indicates the coordinate normal to the flame. A chemical timescale τ_f is then,

$$\tau_\mathrm{f} = \delta_{\mathrm{l}1}/s_\mathrm{l}^0. \tag{A 14}$$

A.2. *Flame curvature, strain rates, and wrinkling*

The flame is identified as an isocontour of a scalar ψ (temperature or reactant mass fraction) yielding a set of N (x_1, x_2) pairs. These are parameterized in terms of arclength s starting at one end of the flame as $(x_1^{(n)}(s^{(n)}), x_2^{(n)}(s^{(n)}))$, $n = 1, 2, \ldots, N$. Local flame curvature $\mathscr{R}^{-1}$ ($\mathscr{R}$ being the radius of curvature) is then calculated as,

$$\mathscr{R}^{-1} = \left\{\left(\frac{\mathrm{d}^2 x_1}{\mathrm{d}s^2}\right)^2 + \left(\frac{\mathrm{d}^2 x_2}{\mathrm{d}s^2}\right)^2\right\}^{\frac{1}{2}}, \tag{A 15}$$

where the derivatives are evaluated using finite differences.

Hydrodynamic strain rates on the flame front are computed differently. The local unit normal vector $\boldsymbol{n}$ and unit tangent vector $\boldsymbol{t}$ to the flame are defined using the gradient of the scalar field ψ directly,

$$\boldsymbol{n} = \nabla\psi/(\nabla\psi\cdot\nabla\psi)^{\frac{1}{2}},$$
$$\boldsymbol{t}\times\boldsymbol{n} = \hat{i}_3, \tag{A 16}$$

where $\hat{i}_3$ is a unit basis vector normal to the (x_1, x_2)-plane for a right-handed coordinate system.

The strain rates normal to and tangent to the flame are then,

$$a_\mathrm{n} = \boldsymbol{nn}:\nabla\boldsymbol{u}, \quad a_\mathrm{t} = \boldsymbol{tt}:\nabla\boldsymbol{u}. \tag{A 17}$$

These satisfy the identity $a_\mathrm{n} + a_\mathrm{t} = \nabla\cdot\boldsymbol{u}$ (Candel & Poinsot 1990).

Scales of flame wrinkling can be defined in many ways. For our purposes, two simple definitions suffice. The largest scale of wrinkling is characterized by the width of the turbulent 'flame brush', that is,

$$l_\mathrm{brush} = \max_{n=1,N}\{x_1^{(n)}(s^{(n)})\} - \min_{n=1,N}\{x_1^{(n)}(s^{(n)})\}. \tag{A 18}$$

The second scale that is introduced is based on the area-weighted flame curvature,

$$l_{\mathscr{R}} = \langle[\mathscr{R}^{-1} - \langle\mathscr{R}^{-1}\rangle]^4\rangle^{-\frac{1}{4}}. \tag{A 19}$$

The high power of curvature emphasizes the smaller scales of flame wrinkling.

REFERENCES

Abraham, J., Williams, F. A. & Bracco, F. V. 1985 A discussion of turbulent flame structure in premixed charges. *SAE Paper no.* 850345.

Ashurst, W. T. 1990 Geometry of premixed flames in three-dimensional turbulence. In *Proc. 1990 Summer Program, Center for Turbulence Research, Stanford University & NASA Ames*, pp. 245–253.

Ashurst, W. T. & Barr, P. K. 1983 Stochastic calculation of laminar wrinkled flame propagation via vortex dynamics. *Combust. Sci. Technol* **34**, 227–256.

Ashurst, W. T., Peters, N. & Smooke, M. D. 1987 Numerical simulation of turbulent flame structure with non-unity Lewis number. *Combust. Sci. Technol.* **53**, 339–375.

Ashurst, W. T., Shivashinsky, G. I. & Yakhot, V. 1988 Flame-front propagation in nonsteady hydrodynamic fields. *Combust. Sci. Technol.* **62**, 273–284.

Batchelor, G. K. 1953 *The Theory of Homogeneous Turbulence.* Cambridge University Press.

Becker, H., Monkhouse, P. B., Wolfrum, J., Cant, R. S., Bray, K. N. C., Maly, R., Pfister, W., Stahl, G. & Warnatz, J. 1990 Investigation of extinction in unsteady flames in turbulent combustion by 2D-LIF of OH radicals and flamelet analysis. *23rd Symp. (Intl) on Combust*, pp. 817–823. The Combustion Institute, Pittsburgh.

BLINT, R. J. 1988 Flammability limits for exhaust gas diluted flames. *22nd (Intl) on Combust.* pp. 1547–1554. The Combustion Institute, Pittsburgh.

BLINT, R. J. 1991 Stretch in premixed laminar flames under IC engine conditions. *Combust. Sci. Technol.* **75**, 115–128.

BRACCO, F. V. 1988 Structure of flames in premixed-charge IC engines. *Combust. Sci. Technol.* **58**, 209–230.

BRAY, K. N. C. 1990 Studies of turbulent burning velocity. *Proc. R. Soc. Lond.* A**431**, 315–335.

BRAY, K. N. C. & LIBBY, P. 1986 Passage times and flamelet crossing frequencies in premixed turbulent combustion. *Combust. Sci. Technol.* **47**, 253–274.

CANDEL, S., MAISTRET, E., DARABIHA, N., POINSOT, T., VEYNANTE, D. & LACAS, F. 1988 Experimental and numerical studies of turbulent ducted flames. *Marble Symp. CALTECH.*

CANDEL, S. M. & POINSOT, T. J. 1990 Flame stretch and the balance equation for the flame area. *Combust. Sci. Technol.* **70**, 1–15.

CANT, R. S. & BRAY, K. N. C. 1988 Strained laminar flamelet calculations of premixed turbulent combustion in a closed vessel. *22nd Symp. (Intl) on Combust.* pp. 791–799. The Combustion Institute, Pittsburgh.

CANT, R. S., POPE, S. B. & BRAY, K. N. C. 1990*a* Modelling of flamelet surface-to-volume ratio in turbulent premixed combustion. *23rd Symp. (Intl) on Combust.* pp. 809–815. The Combustion Institute, Pittsburgh.

CANT, R. S., RUTLAND, C. J. & TROUVÉ, A. 1990*b* Statistics for laminar modeling. In *Proc. 1990 Summer Program, Center for Turbulence Research, Stanford University & NASA Ames*, pp. 271–279.

CHELLIAH, H. K. & WILLIAMS, F. A. 1987 Asymptotic analysis of two-reactant flames with variable properties and Stefan–Maxwell transport. *Combust. Sci. Technol.* **51**, 129–144.

CLAVIN, P. 1985 Dynamic behavior of premixed flame fronts in laminar and turbulent flows. *Prof. Energy Combust. Sci.* **11**, 1–59.

EL TAHRY, S. H. 1990 A turbulence combustion model for premixed charge engines. *Combust. Flame* **79**, 122–140.

EL TAHRY, S. H., RUTLAND, C. J. & FERZIGER, J. H. 1991 Structure and propagation speeds of turbulent premixed flames – a numerical study. *Combust. Flame* **83**, 155–173.

GHONIEM, A. F. & KRISHNAN, A. 1988 Origin and manifestation of flow–combustion interactions in a premixed shear layer. *22nd Symp. (Intl) on Combust.* pp. 665–675. The Combustion Institute, Pittsburgh.

GIRIMAJI, S. S. & POPE, S. B. 1992 Propagating surfaces in isotropic turbulence. *J. Fluid Mech.* **234**, 247–277.

HERRING, J. R., ORSZAG, S. A., KRAICHNAN, R. H. & FOX, D. G. 1974 Decay of two-dimensional homogeneous turbulence. *J. Fluid Mech.* **66**, 417–444.

HINZE, J. O. 1975 *Turbulence*, 2nd edn. McGraw-Hill.

KERSTEIN, A. R., ASHURST, W. T. & WILLIAMS, F. A. 1988 Field equations for interface propagation in an unsteady homogeneous flowfield. *Phys. Rev.* A**37**, 2728–2731.

LEE. T.-W., NORTH, G. L. & SANTAVICCA, D. A. 1991 Curvature and orientation statistics of turbulent premixed flame fronts. *Combust. Sci. Technol.* (submitted). Also presented at Spring 1991 meeting of the Western States Section of the Combustion Institute.

LELE, S. 1990 Compact finite difference schemes with spectral-like resolution. *J. Comput. Phys.* (submitted).

LESIEUR, M. 1987 *Turbulence in Fluids.* Martinus Nijhoff.

MAISTRET, E., DARABIHA, N., POINSOT, T., VEYNANTE, D., LUCAS, F., CANDEL, S. & ESPOSITO, E. 1989 Recent developments in the coherent flame description of turbulent combustion (ed. A. Dervieux & B. Larrouturou). Lecture Notes in Physics. Numerical Combustion, vol. 351.

MANTZARAS, J., FELTON, P. G. & BRACCO, F. V. 1988 Three-dimensional visualization of premixed-charge engine flames. *SAE Paper no.* 881635.

MENEVEAU, C. & POINSOT, T. 1991 Stretching and quenching of flamelets in premixed turbulent combustion. *Combust. Flame* **86**, 311–332.

POINSOT, T. 1991 Flame ignition in a premixed turbulent flow. In *Center for Turbulence Res. Ann. Res. Briefs, Center for Turbulence Research, Stanford University & NASA Ames*, pp. 1–22.

POINSOT, T., ECHEKKI, T. & MUNGAL, M. G. 1992 A study of the laminar flame tip and implications for premixed turbulent combustion. *Combust. Sci. Technol.* **81**, 45–55.

POINSOT, T. & LELE, S. 1992 Boundary conditions for direct simulations of compressible viscous flows. *J. Comput. Phys.* **101**, 104–129. Also CTR Manuscript 102, December 1989, Center for Turbulence Research, Stanford University.

POINSOT, T., VEYNANTE, D. & CANDEL, S. 1990 Diagrams of premixed turbulent combustion based on direct simulation. *23rd Symp. (Intl) on Combust.*, pp. 613–619. The Combustion Institute, Pittsburgh. Also CTR Manuscript 110, June 1990, Center for Turbulence Research, Stanford University.

POINSOT, T., VEYNANTE, D. & CANDEL, S. 1991 Quenching processes and premixed turbulent combustion diagrams. *J. Fluid Mech.* **228**, 561–606.

POPE, S. B. 1988 Evolution of surfaces in turbulence. *Intl J. Engng Sci.* **26**, 445–469.

POPE, S. B. & CHENG, W. 1988 The stochastic flamelet model of turbulent premixed combustion. *22nd Symp. (Intl) on Combust.* pp. 781–789. The Combustion Institute, Pittsburgh.

RUTLAND, C. J., FERZIGER, J. H. & EL TAHRY, S. H. 1990 Full numerical simulation and modeling of turbulent premixed flames. *23rd Symp. (Intl) on Combust.*, pp. 621–627. The Combustion Institute, Pittsburgh.

RUTLAND, C. & TROUVÉ, A. 1990 Premixed flame simulations for nonunity Lewis numbers. In *Proc. 1990 Summer Program, Center for Turbulence Research, Stanford University & NASA Ames*, pp. 299–309.

TENNEKES, H. & LUMLEY, J. L. 1972 *A First Course in Turbulence.* MIT.

WILLIAMS, F. A. 1985 *Combustion Theory*, 2nd edn. Benjamin Cummings.

WRAY, A. 1990 Minimal storage time-advancement schemes for spectral methods. *J. Comput. Phys.* (submitted).

WU, M. S., KWON, S., DRISCOLL, J. F. & FAETH, G. M. 1990 Turbulent premixed hydrogen/air flames at high Reynolds numbers. *Combust. Sci. Technol.* **73**, 327–350.

YEUNG, P. K., GIRIMAJI, S. S. & POPE, S. B. 1990 Straining and scalar dissipation on material surfaces in turbulence: implications for flamelets. *Combust. Flame.* **79**, 340–365.

ZIEGLER, G. F. W., ZETTLITZ, A., MEINHARDT, P., HERWEG, R., MALY, R. & PFISTER, W. 1988 Cycle-resolved two-dimensional flame visualization in a spark-ignition engine. *SAE Paper no.* 881634.